Discrete Transparent Boundary Conditions for Time-Dependent Systems of Schrödinger Equations

A. Zisowsky[1], A. Arnold[2], M. Ehrhardt[1], Th. Koprucki[3]

March 24, 2004

zisowsky@math.tu-berlin.de, anton.arnold@math.uni-muenster.de, ehrhardt@math.tu-berlin.de, koprucki@wias-berlin.de

[1] Institut für Mathematik, Technische Universität Berlin, Str. des 17. Juni 136, D-10623 Berlin

[2] Institut für Numerische Mathematik, Universität Münster, Einsteinstr. 62, D-48149 Münster

[3] Weierstrass-Institut für Angewandte Analysis und Stochastik, Mohrenstr. 39, D-10117 Berlin

AMS 2000 Subject Classification: 65M12, 35Q40, 45K05

Key words: systems of Schrödinger equations, transparent boundary conditions, layered semiconductors, discrete convolution, sum of exponentials, finite difference schemes

Abstract

This work is concerned with *transparent boundary conditions* (TBCs) for *systems of Schrödinger type equations*, namely the time-dependent *kp-Schrödinger equations*. These TBCs have to be constructed for the discrete scheme, in order to maintain stability and to avoid numerical reflections. The discrete transparent boundary conditions (DTBCs) are constructed using the solution of the exterior problem with Laplace and $\mathcal{Z}$-transformation respectively. Hence we will analyse the numerical error caused by the inverse $\mathcal{Z}$-transformation. Since these DTBCs are non-local in time and thus very costly, we present approximate DTBCs, that allow a fast calculation of the boundary terms.

1 Introduction

The operating principle of quantum-electronic semiconductor devices such as resonant tunneling diodes (RTD) [Sin93, Chap. 14] or opto-electronic devices such as quantum-cascade lasers [SKB+98] and multi-quantum-well electro-absorption modulators [DF93] relies on the tunneling process of carriers through barrier structures. Such barrier structures are typically layered semiconductor heterostructures [Sin93], [SKB+98], [DF93] with a barrier thickness of a few nanometer. The transient simulation of wave packets tunneling through such nano-scale semiconductor heterostructures is the key for the understanding of such transport processes [ZG91], [SH91], [SS91]. In particular transient simulations can be used to estimate tunneling times [SS91], charging and

escape times [ZG91], [SH91], or lifetimes of the carriers [DF93], [WM93]. For the simulation of the tunneling process usually a scalar Schrödinger equation defined by BenDaniel-Duke-type Hamiltonians [Bas88, Chap. 3] is used [ZG91], [SS91], [WM93]. The underlying approximation of the electronic band structure of this type of models is that of a single parabolic band. Parabolic single-band approximations are in good agreement with the real band structure in the vicinity of the minima of the conduction bands, that part of the band structure which is usually occupied by the electrons. For the treatment of the holes, occupying the maxima of the valence bands, the accuracy of parabolic single-band models is often not sufficient. This is mainly due to the fact, that the valence bands possess a much more complex band structure [Car96], [Bas88], [CC92], [Chu95], [BAM98], [SS91], [DF93]. However, the electronic states of the holes can be approximated well by *multi-band* states which satisfy a so-called *kp-Schrödinger equation*. The time-dependent *kp*-Schrödinger equation describes the time evolution of the multi-band electronic state and can be regarded as a *linear coupled system* of scalar Schrödinger equations. The evolution is governed by the *kp*-Schrödinger operator which as an extension to the single-band models describes a *system* of bands of the band structure, e.g. the four topmost valence bands [Bas88], [CC92], [Chu95], [BAM98]. There exists a whole bunch of such multi-band *kp*-models [MGO94] including also combined models for conduction and valence bands. The later also allow for a non-parabolic approximation of the conduction bands. For devices where the parabolic conduction band approximation is not sufficient such *kp*-models can be used. For unipolar devices where by crossing a barrier a conduction-band to valence-band transition is possible such as resonant interband tunneling diodes (RITD) or for bipolar devices where additionally the hole tunneling processes are important such as multi-quantum well electro-absorption modulators multi-band modeling is necessary. In this cases the numerical solution of the time-dependent *kp*-Schrödinger equation can be used to understand and to determine the tunneling properties of corresponding semiconductor heterostructures by studying the time evolution of the multi-band electronic state.

In this paper we construct and approximate so called *discrete transparent boundary conditions* (DTBCs) for a time dependent system of the *kp*-Schrödinger-type. Such type of linear systems of Schrödinger-type equations also arise in so-called "parabolic systems" in electromagnetic wave propagation [Lev00]. Artificial BCs have to be imposed to restrict the unbounded domain, on which the differential equation operates, to a finite computational domain. These BCs are called *transparent*, if the solution on the whole space restricted to the computational domain is equal to the solution with the artificial BCs. The artificial boundary splits the problem into three parts: the interesting interior problem and a left and right exterior problem. For constant coefficients the exterior problems can be solved explicitly by Laplace transformation in the continuous and $\mathcal{Z}$-transformation in the discrete case. Claiming C^1-continuity of the solution at the artificial boundaries yields the TBC. The inverse Laplace/$\mathcal{Z}$-transformation involves a convolution in time and yields a non-local in time BC, which is highly precise but very costly. To reduce the numerical effort, we introduce approximate TBCs. Since the inverse $\mathcal{Z}$-transformation must be accomplished numerically, a small error is induced. We scrutinise this critical point in the numerical computation and consider the numerical error.

The paper is organised as follows: Sec. 2 describes the system of Schrödinger equations in

general and presents a quantum well structure with a double barrier as an example, that will be considered throughout this work. We derive the analytic TBC in Sec. 3 and a discrete version in Sec. 4. The DTBC is a discrete convolution. We scrutinise its coefficients, introduce summed coefficients and verify a stability estimate numerically. In Sec. 5 we then explain our strategy to compute the coefficients by a numerical inverse $\mathcal{Z}$-transformation and consider its numerical error. In Sec. 6 we approximate the coefficients by a sum of exponentials ansatz and present a fast evaluation of the approximated DTBC. Finally in Sec. 7 we present our numerical results.

2 The system of *kp*-Schrödinger equations

The equation we consider is a system of *Schrödinger-type equations* in one space dimension, namely the *kp*-Schrödinger equation for one-dimensional semiconductor nanostructures. One-dimensional semiconductor nanostructures are layered *heterostructures* consisting of layers of different semiconductor materials with abrupt, planar heterojunction interfaces between the layers [Sin93]. Typical examples are semiconductor quantum wells and double barrier structures [Sin93], [Bas88], [Chu95]. A widely used approach for the modeling of the near-band-edge electronic states in semiconductor nanostructure is the *kp*-method [Kan82] in combination with the envelope function approximation [Bas88], [Bur92],[Bur94],[Bur98]. Within this approach the electronic state $\Psi(r)$ is approximated in terms of d bands

$$\Psi_{\mathbf{k}_\parallel} = \exp(i\mathbf{k}_\parallel \cdot \mathbf{r}_\parallel) \sum_{\nu=1}^{d} \varphi_\nu(x;\mathbf{k}_\parallel) u_{\nu,\mathbf{k}=0}(r).$$

The index $\parallel$ indicates in-plane vectors and x denotes the growth direction of the semiconductor layers. $\mathbf{k}_\parallel = (k_1, k_2)$ is the reduced wave vector and $u_{\nu,\mathbf{k}=0}(r)$ are lattice periodic, zone-center Bloch functions varying on the atomic scale and $\varphi_\nu(x;\mathbf{k}_\parallel)$ are the corresponding envelope functions describing the variation of the wave function on the nanoscale. The vector of the envelope functions $\boldsymbol{\varphi} = (\varphi_1, \cdots, \varphi_d)$ fulfils the *kp*-Schrödinger equation

$$i\frac{\partial}{\partial t}\boldsymbol{\varphi} = H\Big(\mathbf{k}_\parallel, -i\frac{\partial}{\partial x}\Big)\boldsymbol{\varphi}.$$

There is a hierarchy of *kp*-models [MGO94] describing on the simplest stage the band-mixing between the heavy holes and the light holes by use of a 4×4 Luttinger-Kohn-Hamiltonian [Bas88], [Chu91], [CC92], [Chu95]. Depending on the model Hamiltonian effects such as quantum confinement, band-mixing, spin-orbit interaction and mechanical strain can be treated consistently.

In notation we follow Bandelow, Kaiser, Koprucki and Rehberg, who performed in [BKKR00] a rigorous analysis of spectral properties for the spatially one-dimensional *kp*-Schrödinger operators. The system then reads as follows

$$\begin{aligned} i\frac{\partial}{\partial t}\boldsymbol{\varphi} \;=\; & -\frac{\partial}{\partial x}(\mathbf{m}(x)\frac{\partial}{\partial x}\boldsymbol{\varphi}) + \mathbf{M}_0(x)\frac{\partial}{\partial x}\boldsymbol{\varphi} - \frac{\partial}{\partial x}(\mathbf{M}_0^H(x)\boldsymbol{\varphi}) \\ & + k_1\left(\mathbf{M}_1(x)\frac{\partial}{\partial x}\boldsymbol{\varphi} - \frac{\partial}{\partial x}(\mathbf{M}_1^H(x)\boldsymbol{\varphi})\right) + k_2\left(\mathbf{M}_2(x)\frac{\partial}{\partial x}\boldsymbol{\varphi} - \frac{\partial}{\partial x}(\mathbf{M}_2^H(x)\boldsymbol{\varphi})\right) \\ & + k_1\mathbf{U}_1(x)\boldsymbol{\varphi} + k_2\mathbf{U}_2(x)\boldsymbol{\varphi} + k_1^2\mathbf{U}_{11}(x)\boldsymbol{\varphi} + k_2^2\mathbf{U}_{22}(x)\boldsymbol{\varphi} + k_1k_2(\mathbf{U}_{12}(x) + \mathbf{U}_{21}(x))\boldsymbol{\varphi} \\ & + \mathbf{v}(x)\boldsymbol{\varphi} + \mathbf{e}(x)\boldsymbol{\varphi}, \qquad x \in \mathbb{R}, t > 0, \quad k_1, k_2 \in \mathbb{R}, \end{aligned} \tag{2.1}$$

where $\boldsymbol{\varphi}(x,t) \in \mathbb{C}^d$, the mass matrix $\mathbf{m}(x)$ and $\mathbf{e}(x)$ are real diagonal $d \times d$-matrices. $\mathbf{U}_i(x)$, $\mathbf{U}_{ij}(x)$ and $\mathbf{v}(x)$ are Hermitian $d \times d$-matrices. The $d \times d$-matrices $\mathbf{M}_0(x)$, $\mathbf{M}_1(x)$ and $\mathbf{M}_2(x)$ are skew-Hermitian. $\mathbf{e}(x)$ describes the variation of the band-edges. The band-mixing due to the kp-interaction of the first and second order are described by the terms containing the matrices $\mathbf{M}_\alpha, \mathbf{U}_\alpha, \alpha = 0,1,2$, and $\mathbf{U}_{\alpha\beta}, \alpha, \beta = 1,2$, respectively. The potential $\mathbf{v}$ can cover couplings induced by the spin-orbit interaction or by mechanical strain. Neglecting all non-diagonal coupling terms the system reduces to an uncoupled system of scalar Schrödinger equations corresponding to the case of uncoupled parabolic bands. In this sense the couplings can be interpreted as correction terms to the parabolic band structure approximation.

Since the formulation (2.1) is rather lengthy and we abbreviate the coefficient functions

$$\mathbf{M}_S(x) := \mathbf{M}_0(x) + k_1\mathbf{M}_1(x) + k_2\mathbf{M}_2(x), \tag{2.2a}$$

$$\mathbf{V}(x) := k_1\mathbf{U}_1(x)+k_2\mathbf{U}_2(x)+k_1^2\mathbf{U}_{11}(x)+k_2^2\mathbf{U}_{22}(x)+k_1k_2(\mathbf{U}_{12}(x)+\mathbf{U}_{21}(x))+\mathbf{v}(x)+\mathbf{e}(x). \tag{2.2b}$$

Then $\mathbf{M}_S(x)$ is skew-Hermitian, $\mathbf{V}(x)$ is Hermitian and (2.1) reads

$$i\frac{\partial}{\partial t}\boldsymbol{\varphi} = -\frac{\partial}{\partial x}(\mathbf{m}(x)\frac{\partial}{\partial x}\boldsymbol{\varphi}) + \mathbf{M}_S(x)\frac{\partial}{\partial x}\boldsymbol{\varphi} - \frac{\partial}{\partial x}(\mathbf{M}_S^H(x)\boldsymbol{\varphi}) + \mathbf{V}(x)\boldsymbol{\varphi}, \quad x \in \mathbb{R}, t > 0. \tag{2.3}$$

An important property of the system (2.3) is the constancy in time of $||\boldsymbol{\varphi}||_{L^2}^2$ (conservation of mass). To verify this we multiply (2.3) with $\boldsymbol{\varphi}^H$ from the left:

$$\frac{\partial}{\partial t}||\boldsymbol{\varphi}||_{L^2}^2 = 2\,\mathrm{Im}\left(\int_{\mathbb{R}} \boldsymbol{\varphi}_x^H\mathbf{m}\boldsymbol{\varphi}_x\,dx + \int_{\mathbb{R}} \boldsymbol{\varphi}^H\mathbf{V}\boldsymbol{\varphi}\,dx + \int_{\mathbb{R}} \underbrace{\boldsymbol{\varphi}^H\mathbf{M}_S\boldsymbol{\varphi}_x + \boldsymbol{\varphi}_x^H\mathbf{M}_S^H\boldsymbol{\varphi}}_{\in\mathbb{R}}\,dx\right) = 0.$$

This follows by integration by parts and remembering that $\mathbf{V}$ and $\mathbf{m}$ are Hermitian and thus the imaginary part of the quadratic forms vanishes. The last term is of the form $y + y^H$ which is real.

2.1 The double-barrier stepped quantum-well structure

At this early stage we introduce an example that we will use throughout this work to illustrate in the sequel intermediate results. We consider the $GaAs/AlGaAs$ double-barrier stepped quantum-well structure (DBSQW) introduced in [ZG91]. The variation of the band-edges $e(x)$ is depicted in Fig. 1. For this structure an analysis of the time evolution of wave packets tunneling through the structure has been performed using a scalar Schrödinger equation [ZG91]. We consider the four-band Luttinger-Kohn-Hamiltonian [Bas88], [Chu91], [CC92], [Chu95] modeling the band-mixing heavy holes and the light holes. In atomic units the coefficient matrices for the corresponding 4×4 system of Schrödinger equations are given by:

$$\mathbf{m} = \begin{pmatrix} \gamma & 0 & 0 & 0 \\ 0 & 1 & 0 & 0 \\ 0 & 0 & 1 & 0 \\ 0 & 0 & 0 & \gamma \end{pmatrix}$$

$$\mathbf{M}_1 = -\frac{1}{2}\frac{\gamma_3}{\gamma_1+2\gamma_2}\sqrt{3}i\begin{pmatrix} 0 & -1 & 0 & 0 \\ -1 & 0 & 0 & 0 \\ 0 & 0 & 0 & 1 \\ 0 & 0 & 1 & 0 \end{pmatrix}, \qquad \mathbf{M}_2 = -i\mathbf{M}_1$$

$$\mathbf{U}_{11} = \frac{1}{2}\frac{1}{\gamma_1+2\gamma_2}\begin{pmatrix} \gamma_1+\gamma_2 & 0 & -\sqrt{3}\gamma_2 & 0 \\ 0 & \gamma_1-\gamma_2 & 0 & -\sqrt{3}\gamma_2 \\ -\sqrt{3}\gamma_2 & 0 & \gamma_1-\gamma_2 & 0 \\ 0 & -\sqrt{3}\gamma_2 & 0 & \gamma_1+\gamma_2 \end{pmatrix}$$

$$\mathbf{U}_{22} = \frac{1}{2}\frac{1}{\gamma_1+2\gamma_2}\begin{pmatrix} \gamma_1+\gamma_2 & 0 & \sqrt{3}\gamma_2 & 0 \\ 0 & \gamma_1-\gamma_2 & 0 & \sqrt{3}\gamma_2 \\ \sqrt{3}\gamma_2 & 0 & \gamma_1-\gamma_2 & 0 \\ 0 & \sqrt{3}\gamma_2 & 0 & \gamma_1+\gamma_2 \end{pmatrix}$$

$$\mathbf{U}_{12} + \mathbf{U}_{21} = \frac{1}{\gamma_1+2\gamma_2}\sqrt{3}\gamma_2 i \begin{pmatrix} 0 & 0 & 1 & 0 \\ 0 & 0 & 0 & 1 \\ -1 & 0 & 0 & 0 \\ 0 & -1 & 0 & 0 \end{pmatrix}$$

with $\gamma = \frac{\gamma_1-2\gamma_2}{\gamma_1+2\gamma_2}$. For the values of the band structure parameters $\gamma_1, \gamma_2, \gamma_3$ we take the values of $GaAs$ given by $\gamma_1 = 4 \cdot 6.85$, $\gamma_2 = 4 \cdot 2.1$, $\gamma_3 = 4 \cdot 2.9$. For the in-plane wave-vector $\mathbf{k}_\parallel$ we choose $k_1 = 2.3, k_2 = 0$. As initial condition we use a Gaussian wave packet of spin-up light holes

$$\boldsymbol{\varphi}(x,0) = (2\pi\sigma^2)^{\frac{1}{4}} \exp\left(ik_r x - \frac{(x-x_0)^2}{\sigma^2}\right) \begin{pmatrix} 0 \\ 1 \\ 0 \\ 0 \end{pmatrix}, \tag{2.4}$$

with $\sigma = 3$, $x_0 = -2\sigma$ and $k_r = \sqrt{6.99}$. The band-edge profile of the double-barrier stepped quantum-well is taken from [ZG91] and defined by

$$\mathbf{e}(x) = \begin{cases} 0, & x \leq 22 \\ \frac{25}{2}, & 22 < x \leq 22.5 \\ \frac{5}{2}, & 22.5 < x \leq 23 \\ 0, & 23 < x \leq 23.5 \\ \frac{25}{2}, & 23.5 < x \leq 24 \\ 0, & 24 < x \end{cases}. \tag{2.5}$$

The computational domain is now defined such that it contains the initial data and the important part of the changing potential (cf. Fig. 1). Therefore, we introduce TBCs at the left and right boundary.

3 Transparent boundary conditions

We will now start to derive the analytic transparent boundary conditions for the kp-Schrödinger equation (2.3) at the left $x = x_L$ and right $x = x_R$ boundary. In the scalar case (classical Schrödinger equation of quantum mechanics), the Laplace-transformed equation in the exterior domain can be solved explicitly. Afterwards the solution is inverse transformed, thus yielding

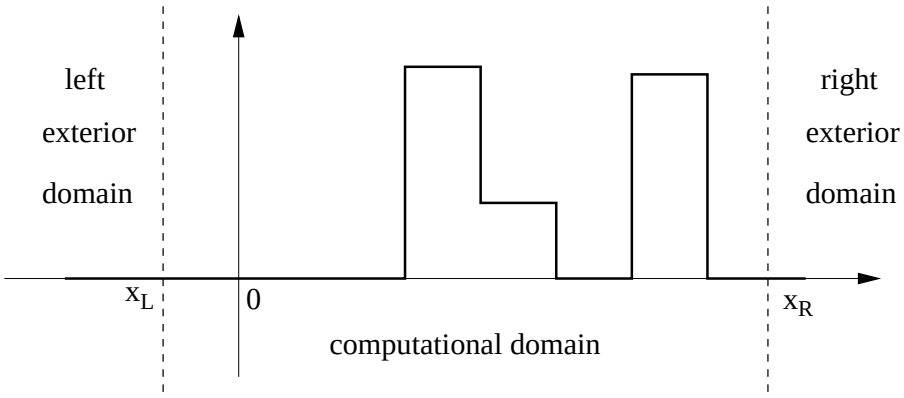

Figure 1: Variation of the band-edge for the $GaAs/AlGaAs$ double-barrier stepped quantum-well structure.

the analytic TBC (cf. [Arn98]). For systems of equations the inverse Laplace transform in general cannot be calculated explicitly. Nevertheless, we will present the derivation of the Laplace transformed TBC and show when it exists.

For the derivation we consider the Schrödinger equation in the left/right exterior domain. A Laplace transformation yields a system of ordinary differential equations, that can be reduced to first order. Then the solution of this system can be given in terms of its eigenvalues and eigenvectors. We will prove, that half of the eigenvalues have positive real parts and thus yield solutions increasing for $x \to \infty$; the other half has negative real parts, yielding decreasing solutions. Demanding that the part of the increasing solutions in the right (and the decreasing solutions in the left) exterior domain vanishes, leads to the transparent boundary conditions.

We consider equation (2.3) in the bounded domain $[x_L, x_R]$ together with TBCs at $x = x_L$ and $x = x_R$. We will denote the constant parameter matrices in the left and right exterior problem by a superscript L and R respectively, when we need to distinguish between the boundaries. But since the derivation for the left and right TBC is equivalent, we focus on the right boundary and omit the superscript R until needed. The TBC at $x = x_R$ is constructed by considering (2.3) with constant coefficients for $x > x_R$, the so called *right exterior problem*

$$i\boldsymbol{\varphi}_t = -\mathbf{m}\boldsymbol{\varphi}_{xx} + i\mathbf{M}\boldsymbol{\varphi}_x + \mathbf{V}\boldsymbol{\varphi}, \qquad x > x_R,\ t > 0, \tag{3.1}$$

where all coefficient matrices are constant and $\mathbf{M} = \mathbf{M}^H$, $\mathbf{V} = \mathbf{V}^H$ and $\mathbf{m}$ is diagonal. The parameters are

$$\begin{aligned} \mathbf{M} &= -i\left(\mathbf{M}_0 - \mathbf{M}_0^H + k_1(\mathbf{M}_1 - \mathbf{M}_1^H) + k_2(\mathbf{M}_2 - \mathbf{M}_2^H)\right) && \text{(3.2a)} \\ &= -i(\mathbf{M}_S - \mathbf{M}_S^H), && \text{(3.2b)} \\ \mathbf{V} &= k_1\mathbf{U}_1 + k_2\mathbf{U}_2 + k_1^2\mathbf{U}_{11} + k_2^2\mathbf{U}_{22} + k_1k_2(\mathbf{U}_{12} + \mathbf{U}_{21}) + \mathbf{v} + \mathbf{e}. && \text{(3.2c)} \end{aligned}$$

Since $\mathbf{M}_S$ is skew-Hermitian, also $\mathbf{M}_S - \mathbf{M}_S^H = 2\mathbf{M}_S$ is skew-Hermitian, thus $\mathbf{M} = -2i\mathbf{M}_S$ is Hermitian.

We now use the Laplace-transformation given by

$$\hat{\boldsymbol{\varphi}}(x,s) = \int_0^\infty e^{-st}\boldsymbol{\varphi}(x,t)\,dt, \quad s = \alpha + i\xi, \quad \alpha > 0, \quad \xi \in \mathbb{R}, \tag{3.3}$$

and obtain from (3.1) the *transformed right exterior problem*

$$\mathbf{m}\hat{\boldsymbol{\varphi}}_{xx} - i\mathbf{M}\hat{\boldsymbol{\varphi}}_x = (\mathbf{V} - is\mathbf{I})\hat{\boldsymbol{\varphi}}, \qquad x > x_R. \tag{3.4}$$

We will address the question of existence and uniqueness at the end of this section in Lem. 3.3.

To derive the transparent boundary condition we define $\boldsymbol{\nu} = \hat{\boldsymbol{\varphi}}$ and $\boldsymbol{\eta} = \hat{\boldsymbol{\varphi}}_x$ and thus reduce the order of the differential equation to obtain a system of first order differential equations

$$\underbrace{\begin{pmatrix} \mathbf{M} & i\mathbf{m} \\ -i\mathbf{m} & \mathbf{0} \end{pmatrix}}_{\mathbf{A}} \begin{pmatrix} \boldsymbol{\nu}_x \\ \boldsymbol{\eta}_x \end{pmatrix} = \underbrace{\begin{pmatrix} i\mathbf{V} + s\mathbf{I} & \mathbf{0} \\ \mathbf{0} & -i\mathbf{m} \end{pmatrix}}_{\mathbf{B}} \begin{pmatrix} \boldsymbol{\nu} \\ \boldsymbol{\eta} \end{pmatrix}, \qquad x > x_R. \tag{3.5}$$

We will show that the matrix $\mathbf{A}^{-1}\mathbf{B}$ is regular, because $\mathbf{A}^{-1}$ and $\mathbf{B}$ are regular. To this end we calculate the determinant of $\mathbf{A}$:

$$\det \begin{pmatrix} \mathbf{M} & i\mathbf{m} \\ -i\mathbf{m} & \mathbf{0} \end{pmatrix} = (-1)^n \det \begin{pmatrix} i\mathbf{m} & \mathbf{M} \\ \mathbf{0} & -i\mathbf{m} \end{pmatrix} = (-1)^n \det(\mathbf{m})^2 \neq 0, \tag{3.6}$$

since the determinant of a block-tridiagonal matrix is the product of the determinants of the block matrices on the diagonal. Here the determinant is obviously nonzero, since $\mathbf{m}$ is regular. Therefore the matrix $\mathbf{A}$ is regular with the inverse

$$\mathbf{A}^{-1} = \mathbf{m}^{-1} \begin{pmatrix} \mathbf{0} & i\mathbf{I} \\ -i\mathbf{I} & -\mathbf{M}\mathbf{m}^{-1} \end{pmatrix} \text{ and } \mathbf{A}^{-1}\mathbf{B} = \begin{pmatrix} \mathbf{0} & \mathbf{I} \\ \mathbf{m}^{-1}(\mathbf{V} - is\mathbf{I}) & i\mathbf{m}^{-1}\mathbf{M} \end{pmatrix}. \tag{3.7}$$

The matrix $\mathbf{B}$ is a block diagonal matrix and thus its eigenvalues are the eigenvalues of the matrices on the diagonal. $\mathbf{V}$ is Hermitian, and thus it is diagonalisable and its eigenvalues $\upsilon_1, \ldots, \upsilon_d$ are real. Then $i\mathbf{V} + s\mathbf{I}$ is similar to $\operatorname{diag}(\alpha + (\upsilon_1 + \xi)i, \ldots, \alpha + (\upsilon_n + \xi)i)$ which is regular for $\operatorname{Re}(s) = \alpha > 0$, $s = \alpha + i\xi$, $\xi \in \mathbb{R}$. Therefore, $\mathbf{A}^{-1}\mathbf{B}$ as a product of regular matrices is regular for $\operatorname{Re}(s) > 0$.

We now transform $\mathbf{A}^{-1}\mathbf{B}$ into Jordan form with $\mathbf{A}^{-1}\mathbf{B} = \mathbf{P}\mathbf{J}\mathbf{P}^{-1}$, where $\mathbf{P}^{-1}$ contains the left eigenvectors in rows. We sort the Jordan blocks in $\mathbf{J}$ with respect to an increasing real part of the corresponding eigenvalue. Thus $\mathbf{J}$ can be written as $\mathbf{J} = \left(\begin{smallmatrix} \mathbf{J}_1 & \mathbf{0} \\ \mathbf{0} & \mathbf{J}_2 \end{smallmatrix}\right)$, where $\mathbf{J}_1$ holds all Jordan blocks to eigenvalues with negative real parts and $\mathbf{J}_2$ those with positive real parts. Due to Thm. 3.1 $\mathbf{J}_1$ and $\mathbf{J}_2$ are $d \times d$-matrices. With $\mathbf{P}^{-1} = \left(\begin{smallmatrix} \mathbf{P}_1 & \mathbf{P}_2 \\ \mathbf{P}_3 & \mathbf{P}_4 \end{smallmatrix}\right)$ equation (3.5) can be written as

$$\mathbf{P}^{-1} \begin{pmatrix} \boldsymbol{\nu}_x \\ \boldsymbol{\eta}_x \end{pmatrix} = \begin{pmatrix} \mathbf{J}_1 & \mathbf{0} \\ \mathbf{0} & \mathbf{J}_2 \end{pmatrix} \begin{pmatrix} \mathbf{P}_1 & \mathbf{P}_2 \\ \mathbf{P}_3 & \mathbf{P}_4 \end{pmatrix} \begin{pmatrix} \boldsymbol{\nu} \\ \boldsymbol{\eta} \end{pmatrix} = \begin{pmatrix} \mathbf{J}_1 & \mathbf{0} \\ \mathbf{0} & \mathbf{J}_2 \end{pmatrix} \begin{pmatrix} \mathbf{P}_1\boldsymbol{\nu} + \mathbf{P}_2\boldsymbol{\eta} \\ \mathbf{P}_3\boldsymbol{\nu} + \mathbf{P}_4\boldsymbol{\eta} \end{pmatrix}, \qquad x > x_R. \tag{3.8}$$

Obviously, the upper equation yields parts of the solution, which decrease for $x \to \infty$ and increase for $x \to -\infty$. The opposite is true for the lower equation. We define the *left exterior problem* for $x < x_L$ analogous to the right exterior problem. Then, an equation analogous to (3.8) holds: the *transformed transparent boundary conditions* for the left (a) and right (b) boundary is obtained by extinguishing the respectively increasing parts of the exterior solutions:

$$\mathbf{P}_2^L \hat{\boldsymbol{\varphi}}_x(x_L, s) = -\mathbf{P}_1^L \hat{\boldsymbol{\varphi}}(x_L, s), \tag{3.9a}$$

$$\mathbf{P}_4^R \hat{\boldsymbol{\varphi}}_x(x_R, s) = -\mathbf{P}_3^R \hat{\boldsymbol{\varphi}}(x_R, s). \tag{3.9b}$$

If the matrices $\mathbf{P}_2^L$ and $\mathbf{P}_4^R$ are regular, then the Laplace-transformed TBC can be written in *Dirichlet-to-Neumann form*. It is not clear, if these matrices are regular in general, but for our example this applies for all tested s.

In order to examine if solutions of (3.4) increase or decay, we state the following theorem:

Theorem 3.1 (Splitting Theorem). *For $Re(s) > 0$ the regular matrix $\mathbf{A}^{-1}\mathbf{B}$ has d eigenvalues with positive real part and d with negative real part.*

The proof of this theorem will be obtained as a conclusion of Lem. 3.1 and Lem. 3.2. We first recall the definition of the *inertia* of a matrix $\mathbf{M}$:

Definition 3.1 ([HJ99b]). *The* inertia *of a complex matrix $\mathbf{M}$ is the ordered triple*

$$i(\mathbf{M}) = (i_+(\mathbf{M}), i_-(\mathbf{M}), i_0(\mathbf{M})). \tag{3.10}$$

Here $i_+(\mathbf{M})$, $i_-(\mathbf{M})$ and $i_0(\mathbf{M})$ are the numbers of eigenvalues of $\mathbf{M}$ with resp. positive, negative and zero real part, all counting multiplicity.

Lemma 3.1 (Lemma 2 in [CS63]). *Let $\mathbf{F}, \mathbf{G}$ be $d \times d$-matrices with $\mathbf{G}$ Hermitian and regular, suppose $\mathbf{H} := \mathbf{GF} + \mathbf{F}^H\mathbf{G}$ is positive semi-definite and $i_0(\mathbf{F}) = 0$. Then $i(\mathbf{F}) = i(\mathbf{G})$.*

In order to apply this lemma to $\mathbf{G} := \mathbf{A}$ and $\mathbf{F} := \mathbf{A}^{-1}\mathbf{B}$ we check the assumptions: Since $\mathbf{M}$ is Hermitian, $\mathbf{A} = \mathbf{A}^H$ as well. We already showed, that $\mathbf{A}$ is regular. Then $\mathbf{H}$ satisfies:

$$\begin{aligned} \mathbf{H} &= \mathbf{GF} + \mathbf{F}^H\mathbf{G} = \mathbf{A}(\mathbf{A}^{-1}\mathbf{B}) + \mathbf{B}^H(\mathbf{A}^{-1})^H\mathbf{A}^H \\ &= \mathbf{B} + \mathbf{B}^H = \begin{pmatrix} 2\mathrm{Re}(s)\mathbf{I} & \mathbf{0} \\ \mathbf{0} & \mathbf{0} \end{pmatrix} \geq 0. \end{aligned} \tag{3.11}$$

It remains to show, that $i_0(\mathbf{A}^{-1}\mathbf{B}) = 0$. To this end we prove the following lemma:

Lemma 3.2. *For $Re(s) > 0$ the matrix $\mathbf{A}^{-1}\mathbf{B}$ has no purely imaginary eigenvalues.*

Proof. We assume that $i\lambda$ with $\lambda \in \mathbb{R}$ is eigenvalue of $\mathbf{A}^{-1}\mathbf{B}$. In that case $\hat{\boldsymbol{\varphi}}(x) = \check{\boldsymbol{\varphi}} e^{i\lambda x}$ is a solution of (3.4) and yields for $s = a + i\xi$

$$is\check{\boldsymbol{\varphi}} = (i\alpha - \xi)\check{\boldsymbol{\varphi}} = (\mathbf{m}\lambda^2 - \mathbf{M}\lambda + V)\check{\boldsymbol{\varphi}}. \tag{3.12}$$

This means, that $i\alpha - \xi$ is an eigenvalue of $\mathbf{m}\lambda^2 - \mathbf{M}\lambda + V$. But since $\mathbf{m}\lambda^2 - \mathbf{M}\lambda + V$ is - as a sum of Hermitian matrices - again Hermitian, all its eigenvalues must be real, and therefore $\alpha = 0$ which is a contradiction. □

Conclusion 3.2. *For any eigenvalue λ of $\mathbf{A}^{-1}\mathbf{B}$, $Re(\lambda) = 0$ implies $\lambda = 0$. Thus, since $\mathbf{A}^{-1}\mathbf{B}$ is regular, we have $i_0(\mathbf{A}^{-1}\mathbf{B}) = 0$.*

Hence, Lem. 3.1 applies and yields $i(\mathbf{A}^{-1}\mathbf{B}) = i(\mathbf{A})$. To prove Thm. 3.1, it finally remains to verify that d eigenvalues of $\mathbf{A}$ have positive and d have negative real parts. Therefore we will use a continuity argument: we consider the matrix

$$\mathbf{A}(\varepsilon) := \begin{pmatrix} \varepsilon\mathbf{M} & i\mathbf{m} \\ -i\mathbf{m} & \mathbf{0} \end{pmatrix}, \qquad \varepsilon \in [0, 1]. \tag{3.13}$$

$\mathbf{A}(0)$ has d positive and d negative eigenvalues, which are given by

$$\lambda^0_{2k-1} = m_{k,k} \text{ and } \lambda^0_{2k} = -m_{k,k}, \qquad k = 1, \ldots, d. \tag{3.14}$$

Furthermore for all $\varepsilon \in [0,1]$ the matrix $\mathbf{A}(\varepsilon)$ has no zero eigenvalue (cf. 3.6). Then for ε from zero to one d eigenvalues of $\mathbf{A}(\varepsilon)$ are positive and d are negative, since the eigenvalues are continuous in ε.

Thus, $i(\mathbf{A}) = (d, d, 0)$ holds and with Lem. 3.1 follows $i(\mathbf{A}^{-1}\mathbf{B}) = (d, d, 0)$, if $\mathrm{Re}(s) > 0$, which finishes the proof of Thm. 3.1.

In this section we derived a transparent boundary condition using the solution of the exterior problem. It finally remains to discuss the existence and uniqueness of this solution:

Lemma 3.3. (Existence and uniqueness of the solution to the Laplace-transformed exterior problem).

a) If the solution of the boundary value problem (3.4) *with the boundary data*

$$\hat{\boldsymbol{\varphi}}(x = x_R) = \hat{\boldsymbol{\varphi}}_R, \qquad \hat{\boldsymbol{\varphi}}(x = \infty) = \mathbf{0} \tag{3.15}$$

exists, it is unique for Re(s) sufficiently large.

b) If the block submatrix $\boldsymbol{\mathcal{P}}_1$ *of* $\mathbf{P} = \begin{pmatrix} \boldsymbol{\mathcal{P}}_1 & \boldsymbol{\mathcal{P}}_2 \\ \boldsymbol{\mathcal{P}}_3 & \boldsymbol{\mathcal{P}}_4 \end{pmatrix}$ *is regular, then the solution exists.*

Proof. a) To prove uniqueness we assume, that there exist two such solutions of (3.4),(3.15) $\hat{\boldsymbol{\varphi}}_1$ and $\hat{\boldsymbol{\varphi}}_2$. Then the difference $\hat{\boldsymbol{\varphi}} = \hat{\boldsymbol{\varphi}}_1 - \hat{\boldsymbol{\varphi}}_2$ is a solution of (3.4) with homogeneous boundary data. Multiplying (3.4) with $\hat{\boldsymbol{\varphi}}^H$ from the left and integrating from x_R to ∞ yields after integrating by parts

$$-\int_{x_R}^{\infty} \hat{\boldsymbol{\varphi}}_x^H \mathbf{m} \hat{\boldsymbol{\varphi}}_x dx - i\int_{x_R}^{\infty} \hat{\boldsymbol{\varphi}}^H \mathbf{M} \hat{\boldsymbol{\varphi}}_x dx + \int_{x_R}^{\infty} is|\hat{\boldsymbol{\varphi}}|^2 dx - \int_{x_R}^{\infty} \hat{\boldsymbol{\varphi}}^H \mathbf{V} \hat{\boldsymbol{\varphi}} dx = 0. \tag{3.16}$$

Taking imaginary parts simplifies this, because the quadratic forms of the Hermitian matrices are purely real. Furthermore, we denote $\mathbf{M} = (\mu_{k,l})_{k,l=1}^{d}$ and get

$$\begin{aligned}
0 &= -\int_{x_R}^{\infty} \mathrm{Re}(\hat{\boldsymbol{\varphi}}^H \mathbf{M} \hat{\boldsymbol{\varphi}}_x) dx + \int_{x_R}^{\infty} \mathrm{Re}(s)|\hat{\boldsymbol{\varphi}}|^2 dx \\
&= -\int_{x_R}^{\infty} \sum_{k=1}^{d} \mathrm{Re}(\bar{\hat{\varphi}}_k \mu_{k,k} \hat{\varphi}_{kx}) dx - \int_{x_R}^{\infty} \sum_{k=1}^{d} \sum_{\substack{l=1 \\ l\neq k}}^{d} \mathrm{Re}(\bar{\hat{\varphi}}_k \mu_{k,l} \hat{\varphi}_{lx}) dx + \int_{x_R}^{\infty} \mathrm{Re}(s)|\hat{\boldsymbol{\varphi}}|^2 dx \\
&= -\frac{1}{2}\int_{x_R}^{\infty} \sum_{k=1}^{d} \mu_{k,k} \partial_x |\hat{\varphi}_k|^2 dx - \int_{x_R}^{\infty} \sum_{k=1}^{d} \sum_{l=k+1}^{d} \mathrm{Re}(\bar{\hat{\varphi}}_k \mu_{k,l} \hat{\varphi}_{lx} + \bar{\hat{\varphi}}_l \bar{\mu}_{l,k} \hat{\varphi}_{kx}) dx + \int_{x_R}^{\infty} \mathrm{Re}(s)|\hat{\boldsymbol{\varphi}}|^2 dx \\
&= \int_{x_R}^{\infty} \mathrm{Re}(s)|\hat{\boldsymbol{\varphi}}|^2 dx \geq 0 \qquad \text{for } \mathrm{Re}(s) > 0,
\end{aligned}$$

because $\partial_x|\hat{\varphi}_k|^2 = \bar{\hat{\varphi}}_{kx}\hat{\varphi}_k + \bar{\hat{\varphi}}_k\hat{\varphi}_{kx} = 2\mathrm{Re}(\bar{\hat{\varphi}}_k\hat{\varphi}_{kx})$ and with partial integration $\int \mu_{k,l}\bar{\hat{\varphi}}_k\hat{\varphi}_{lx} + \int \bar{\mu}_{l,k}\bar{\hat{\varphi}}_l\hat{\varphi}_{kx} = 2\int \mathrm{Im}(\mu_{k,l}\bar{\hat{\varphi}}_k\hat{\varphi}_{lx})$, since $\mathbf{M}$ is Hermitian. From this we conclude $\hat{\boldsymbol{\varphi}} \equiv \mathbf{0}$, which is a contradiction to our assumption.

b) A general solution of (3.5) is given by

$$\begin{pmatrix}\boldsymbol{\nu}\\ \boldsymbol{\eta}\end{pmatrix}(x) = e^{\mathbf{A}^{-1}\mathbf{B}x}\tilde{\mathbf{c}} = \mathbf{P}e^{\mathbf{J}x}\mathbf{P}^{-1}\tilde{\mathbf{c}} = \mathbf{P}e^{\mathbf{J}x}\mathbf{c} = \begin{pmatrix}\boldsymbol{\mathcal{P}}_1 & \boldsymbol{\mathcal{P}}_2\\ \boldsymbol{\mathcal{P}}_3 & \boldsymbol{\mathcal{P}}_4\end{pmatrix}\begin{pmatrix}e^{\mathbf{J}_1 x} & \mathbf{0}\\ \mathbf{0} & e^{\mathbf{J}_2 x}\end{pmatrix}\begin{pmatrix}\mathbf{c}_1\\ \mathbf{c}_2\end{pmatrix}, \quad x > x_R. \tag{3.17}$$

To fulfil the decaying condition $\hat{\boldsymbol{\varphi}}(x) \to \mathbf{0} \quad (x \to \infty)$ the constant $\mathbf{c}_2$ is chosen as zero. Thus the general solution to (3.4) is given by $\hat{\boldsymbol{\varphi}}(x) = \boldsymbol{\mathcal{P}}_1 e^{\mathbf{J}_1 x}\mathbf{c}_1$. The constant $\mathbf{c}_1$ can be determined by the boundary condition $\hat{\boldsymbol{\varphi}}(x_R) = \hat{\boldsymbol{\varphi}}_R$, if the matrix $\boldsymbol{\mathcal{P}}_1$ is regular . Thus, for regular $\boldsymbol{\mathcal{P}}_1$ the existence of a solution to the exterior problem is guaranteed. □

We confirmed the regularity of $\boldsymbol{\mathcal{P}}_1$ for the quantum well for $s = \alpha + i\xi$, where α runs from 0.1 to 100 and ξ from -1000 to 1000 each with steps of 1/10.

4 Discrete transparent boundary conditions

We do not discretise equation (3.9) (by a numerical inverse Laplace transformation), but derive discrete TBCs for a discretisation of (2.3). For the discretisation we choose a uniform grid with the step sizes Δx in space and Δt in time: $x_j = X_L + j\Delta x, t_n = n\Delta t$ with $j = 0, \ldots, J$, $n = 0, \ldots, N$. We discretise (2.3) using the Crank-Nicolson scheme in time and the central differences for the first and second spatial derivatives. The *discrete kp-Schrödinger equation* then reads

$$i\frac{\Delta x^2}{\Delta t}(\boldsymbol{\varphi}_j^{n+1} - \boldsymbol{\varphi}_j^n) = -\Delta^0_{\frac{\Delta x}{2}}(\mathbf{m}_j\Delta^0_{\frac{\Delta x}{2}}\boldsymbol{\varphi}_j^{n+\frac{1}{2}}) + \mathbf{M}_{Sj}\Delta^0\boldsymbol{\varphi}_j^{n+\frac{1}{2}} - \Delta^0(\mathbf{M}_{Sj}^H\boldsymbol{\varphi}_j^{n+\frac{1}{2}}) + V_j\boldsymbol{\varphi}_j^{n+\frac{1}{2}} \tag{4.1}$$

for $j = 1, \ldots, J-1$ and $n = 0, \ldots, N$ with the difference operators

$$\Delta^0_{\frac{\Delta x}{2}}\boldsymbol{\varphi}_j^n = \boldsymbol{\varphi}^n_{j+\frac{1}{2}} - \boldsymbol{\varphi}^n_{j-\frac{1}{2}}, \tag{4.2a}$$

$$\Delta^0\boldsymbol{\varphi}_j^n = (\Delta^+ + \Delta^-)\boldsymbol{\varphi}_j^n = \boldsymbol{\varphi}^n_{j+1} - \boldsymbol{\varphi}^n_{j-1} \tag{4.2b}$$

and $\boldsymbol{\varphi}_j^{n+\frac{1}{2}} = \frac{\boldsymbol{\varphi}_j^{n+1}+\boldsymbol{\varphi}_j^n}{2}$. With $\triangle_t^+$ we will denote the forward difference in time.

An appropriate discretisation scheme should carry over properties of the continuous equation to the difference equation. This is the case for the Crank-Nicolson scheme: it conserves the whole-space l^2-norm and thus it is unconditionally stable for the whole-space problem. To see this, we use (4.1) with summation by parts

$$\begin{aligned}\frac{\Delta x^2}{\Delta t}\triangle_t^+||\boldsymbol{\varphi}^n||_{l^2}^2 &= = 2\frac{\Delta x^2}{\Delta t}\mathrm{Im}\left(\sum_{j=-\infty}^{\infty} i\left(\boldsymbol{\varphi}_j^{n+\frac{1}{2}}\right)^H \triangle_t^+\boldsymbol{\varphi}_j^n\right)\\ &= 2\mathrm{Im}\left(\sum_{j=-\infty}^{\infty}\left(\triangle^0_{\frac{\Delta x}{2}}\boldsymbol{\varphi}_j^{n+\frac{1}{2}}\right)^H\mathbf{m}_j\triangle^0_{\frac{\Delta x}{2}}\boldsymbol{\varphi}_j^{n+\frac{1}{2}} + \sum_{j=-\infty}^{\infty}\left(\boldsymbol{\varphi}_j^{n+\frac{1}{2}}\right)^H\mathbf{V}_j\boldsymbol{\varphi}_j^{n+\frac{1}{2}}\right.\\ &\quad \left. + \sum_{j=-\infty}^{\infty}\left(\boldsymbol{\varphi}_j^{n+\frac{1}{2}}\right)^H\mathbf{M}_{Sj}\triangle^0\boldsymbol{\varphi}_j^{n+\frac{1}{2}} + \sum_{j=-\infty}^{\infty}\left(\left(\boldsymbol{\varphi}_j^{n+\frac{1}{2}}\right)^H\mathbf{M}_{Sj}\triangle^0\boldsymbol{\varphi}_j^{n+\frac{1}{2}}\right)^H\right) = 0,\end{aligned} \tag{4.3}$$

because the matrices $\mathbf{m}_j$ and $\mathbf{V}_j$ are Hermitian. Thus, for the whole-space problem the discrete l^2-norm is constant in time.

For the case of a scalar Schrödinger equation Arnold [Arn98] derived a discrete transparent boundary condition. This DTBC is reflection-free compared to the discrete whole-space solution and conserves the stability properties of the whole-space Crank-Nicolson scheme. The DTBC has the form of a discrete convolution. The convolution coefficients are a function of Legendre polynomials but can be obtained more easily by a three-term recurrence formula. Ehrhardt and Arnold showed in [EA01], that the imaginary parts of the convolution coefficients are not decaying and therefore introduced summed coefficients. We will here use an assimilated method: To derive the DTBC for (4.1) we solve the $\mathcal{Z}$-transformed system of ordinary difference equations in the exterior domain. Then all its solutions are determined by eigenvalues and eigenvectors, which can be distinguished into decaying and increasing solutions by the absolute value of the involved eigenvalue. We obtain the DTBC by claiming, that no influence of increasing solutions exists.

In the exterior space $j \geq J$ ($x_J = x_R$) the parameter matrices are constant and the Crank-Nicolson scheme (4.1) simplifies to

$$i\frac{\Delta x^2}{\Delta t}(\boldsymbol{\varphi}_j^{n+1} - \boldsymbol{\varphi}_j^n) = -\mathbf{m}\Delta^+\Delta^-\boldsymbol{\varphi}_j^{n+1/2} + i\Delta x\mathbf{M}\frac{1}{2}(\Delta^+ + \Delta^-)\boldsymbol{\varphi}_j^{n+1/2} + \Delta x^2\mathbf{V}\boldsymbol{\varphi}_j^{n+1/2} \tag{4.4}$$

for $j \geq J$ and $n \geq 0$. The $\mathcal{Z}$-transformation given by

$$\mathcal{Z}\{\boldsymbol{\varphi}_j^n\} = \hat{\boldsymbol{\varphi}}_j(z) := \sum_{n=0}^{\infty} z^{-n}\boldsymbol{\varphi}_j^n, \qquad z \in \mathbb{C}, \qquad |z| > 1, \tag{4.5}$$

transforms (4.4) to

$$2i\frac{\Delta x^2}{\Delta t}\frac{z-1}{z+1}\hat{\boldsymbol{\varphi}}_j = -\mathbf{m}\Delta^+\Delta^-\hat{\boldsymbol{\varphi}}_j + i\Delta x\mathbf{M}\frac{1}{2}(\Delta^+ + \Delta^-)\hat{\boldsymbol{\varphi}}_j + \Delta x^2\mathbf{V}\hat{\boldsymbol{\varphi}}_j, \qquad j \geq J. \tag{4.6}$$

Lemma 4.1. *If the solution of the $\mathcal{Z}$-transformed exterior problem* (4.6) *with the boundary data*

$$\hat{\boldsymbol{\varphi}}_{j=J} = \hat{\boldsymbol{\varphi}}_J, \qquad \hat{\boldsymbol{\varphi}}_\infty = 0 \tag{4.7}$$

exists, it is unique.

Proof. We assume, that there exist two solutions of (4.6), (4.7) $\hat{\boldsymbol{\varphi}}_1$ and $\hat{\boldsymbol{\varphi}}_2$. The difference $\hat{\boldsymbol{\varphi}} = \hat{\boldsymbol{\varphi}}_1 - \hat{\boldsymbol{\varphi}}_2$ is then a solution of (4.6) with homogeneous boundary data. For this solution $\hat{\boldsymbol{\varphi}}$ we consider (4.6) multiplied by $\hat{\boldsymbol{\varphi}}_j^H$ from the left and take imaginary parts:

$$\begin{aligned} 0 &= \mathrm{Im}\left(2i\frac{\Delta x^2}{\Delta t}\frac{z-1}{z+1}\sum_{j=J}^{\infty}|\hat{\boldsymbol{\varphi}}_j|^2 + \sum_{j=J}^{\infty}\hat{\boldsymbol{\varphi}}_j^H\mathbf{m}\triangle^+\triangle^-\hat{\boldsymbol{\varphi}}_j\right. \\ &\quad \left. -\frac{1}{2}i\Delta x\sum_{j=J}^{\infty}\hat{\boldsymbol{\varphi}}_j^H\mathbf{M}\left(\triangle^+ + \triangle^-\right)\hat{\boldsymbol{\varphi}}_j - \Delta x^2\sum_{j=J}^{\infty}\hat{\boldsymbol{\varphi}}_j^H\mathbf{V}\hat{\boldsymbol{\varphi}}_j\right) \\ &= 2\frac{\Delta x^2}{\Delta t}\mathrm{Re}\left(\frac{z-1}{z+1}\right)\sum_{j=J}^{\infty}|\hat{\boldsymbol{\varphi}}_j|^2 + \mathrm{Im}\left(-\sum_{j=J}^{\infty}\triangle^-\hat{\boldsymbol{\varphi}}_j^H\mathbf{m}\triangle^-\hat{\boldsymbol{\varphi}}_j\right. \\ &\quad \left. -\frac{1}{2}i\Delta x\sum_{j=J}^{\infty}\hat{\boldsymbol{\varphi}}_j^H\mathbf{M}\triangle^-\hat{\boldsymbol{\varphi}}_j + \frac{1}{2}i\Delta x\sum_{j=J}^{\infty}\left(\hat{\boldsymbol{\varphi}}_j^H\mathbf{M}\triangle^-\hat{\boldsymbol{\varphi}}_j\right)^H\right) \geq 0, \end{aligned} \tag{4.8}$$

if $|z|>1$, (because $\mathrm{Re}\left(\frac{z-1}{z+1}\right)=\frac{|z|^2-1}{|z+1|^2}$) and even strictly larger than zero, if $\sum_{j=J}^{\infty}|\hat{\boldsymbol{\varphi}}_j|^2\neq 0$. But this is a contradiction. □

Remark 4.1. *Analogously to the continuous problem the existence of a solution is guaranteed by the regularity of the $S\times S$ principal submatrix of the matrix of right eigenvectors (cf. Lem. 3.3), which holds for our example.*

We proceed to solve the $\mathcal{Z}$-transformed exterior problem and define $\hat{\boldsymbol{\xi}}_j=\Delta^-\hat{\boldsymbol{\varphi}}_j$ to reduce the order of the difference equation (4.6)

$$\begin{pmatrix} i\frac{\Delta x}{2}\mathbf{M} & -\mathbf{m} \\ -\mathbf{I} & \mathbf{I}\end{pmatrix}\begin{pmatrix}\Delta^+\hat{\boldsymbol{\varphi}}_j\\ \Delta^+\hat{\boldsymbol{\xi}}_j\end{pmatrix}=\begin{pmatrix}\Delta x^2 2\frac{z-1}{z+1}\frac{1}{\Delta t}i\mathbf{I}-\Delta x^2\mathbf{V} & -i\frac{\Delta x}{2}\mathbf{M}\\ \mathbf{0} & -\mathbf{I}\end{pmatrix}\begin{pmatrix}\hat{\boldsymbol{\varphi}}_j\\ \hat{\boldsymbol{\xi}}_j\end{pmatrix}, \tag{4.9}$$

i.e.

$$\begin{pmatrix}\Delta^+\hat{\boldsymbol{\varphi}}_j\\ \Delta^+\hat{\boldsymbol{\xi}}_j\end{pmatrix}=\mathbf{A}^{-1}\mathbf{B}\begin{pmatrix}\hat{\boldsymbol{\varphi}}_j\\ \hat{\boldsymbol{\xi}}_j\end{pmatrix}\qquad\text{or}\qquad\begin{pmatrix}\hat{\boldsymbol{\varphi}}_{j+1}\\ \hat{\boldsymbol{\xi}}_{j+1}\end{pmatrix}=(\mathbf{A}^{-1}\mathbf{B}+\mathbf{I})\begin{pmatrix}\hat{\boldsymbol{\varphi}}_j\\ \hat{\boldsymbol{\xi}}_j\end{pmatrix}. \tag{4.10}$$

The regularity of $\mathbf{A}$ will follow from Thm. 4.2.

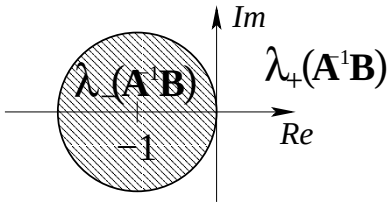

Solutions of (4.6), that are constructed with an eigenvalue λ of $\mathbf{A}^{-1}\mathbf{B}$, are decaying for $x\to\infty$ if $|\lambda+1|<1$ and increasing if $|\lambda+1|>1$.

Analogously to Thm. 3.1 we prove a splitting property of $\mathbf{A}^{-1}\mathbf{B}+\mathbf{I}$:

Theorem 4.2 (Discrete Splitting Theorem). *d of the $2d$ eigenvalues of $\mathbf{A}^{-1}\mathbf{B}+\mathbf{I}$ have an absolute value larger than unity and d have a smaller absolute value, if $|z|\neq 1$.*

A proof of Thm. 4.2 will be given succeeding to the DTBC at the end of this section.

If the eigenvalues $\lambda_1,\ldots,\lambda_{2d}$ of $\mathbf{A}^{-1}\mathbf{B}$ split into two commensurate groups, then the solutions involving those with $|\lambda_k+1|<1$ for $k=1,\ldots,d$ decay for $j\to\infty$ and those with $|\lambda_k+1|>1$ for $k=d,\ldots,2d$ decay for $j\to-\infty$. Thus, we may again split the Jordan form $\mathbf{J}=\left(\begin{smallmatrix}\mathbf{J}_1 & \mathbf{0}\\ \mathbf{0} & \mathbf{J}_2\end{smallmatrix}\right)$ of $\mathbf{A}^{-1}\mathbf{B}+\mathbf{I}$, $\mathbf{J}_1$ containing the Jordan blocks corresponding to solutions decaying for $j\to\infty$ and $\mathbf{J}_2$ those which increase. With the matrix of left eigenvectors $\mathbf{P}^{-1}=\left(\begin{smallmatrix}\mathbf{P}_1 & \mathbf{P}_2\\ \mathbf{P}_3 & \mathbf{P}_4\end{smallmatrix}\right)$ the equation

$$\begin{aligned}\mathbf{P}^{-1}\begin{pmatrix}\hat{\boldsymbol{\varphi}}_{j+1}\\ \hat{\boldsymbol{\xi}}_{j+1}\end{pmatrix} &= \mathbf{P}^{-1}(\mathbf{A}^{-1}\mathbf{B}+\mathbf{I})\begin{pmatrix}\hat{\boldsymbol{\varphi}}_j\\ \hat{\boldsymbol{\xi}}_j\end{pmatrix}=\mathbf{P}^{-1}\mathbf{P}\begin{pmatrix}\mathbf{J}_1 & \mathbf{0}\\ \mathbf{0} & \mathbf{J}_2\end{pmatrix}\begin{pmatrix}\mathbf{P}_1 & \mathbf{P}_2\\ \mathbf{P}_3 & \mathbf{P}_4\end{pmatrix}\begin{pmatrix}\hat{\boldsymbol{\varphi}}_j\\ \hat{\boldsymbol{\xi}}_j\end{pmatrix}\\ &= \begin{pmatrix}\mathbf{J}_1 & \mathbf{0}\\ \mathbf{0} & \mathbf{J}_2\end{pmatrix}\begin{pmatrix}\mathbf{P}_1\hat{\boldsymbol{\varphi}}_j+\mathbf{P}_2\hat{\boldsymbol{\xi}}_j\\ \mathbf{P}_3\hat{\boldsymbol{\varphi}}_j+\mathbf{P}_4\hat{\boldsymbol{\xi}}_j\end{pmatrix}\end{aligned} \tag{4.11}$$

holds and the *transformed discrete transparent boundary conditions* read

$$\mathbf{P}_1^L\hat{\boldsymbol{\varphi}}_1+\mathbf{P}_2^L\hat{\boldsymbol{\xi}}_1=0, \tag{4.12a}$$

$$\mathbf{P}_3^R\hat{\boldsymbol{\varphi}}_J+\mathbf{P}_4^R\hat{\boldsymbol{\xi}}_J=0 \tag{4.12b}$$

for the left (a) and right (a) boundary respectively.

Remark 4.3. *In the considered example the matrices* $\mathbf{P}_1^R, \ldots, \mathbf{P}_4^R$ *and* $\mathbf{P}_1^L, \ldots, \mathbf{P}_4^L$ *were regular, but this is not clear in general.*

For regular matrices $\mathbf{P}_4^R$ and $\mathbf{P}_2^L$ the $\mathcal{Z}$-transformed DTBC can be given in Dirichlet-to-Neumann form

$$\Delta^- \hat{\boldsymbol{\varphi}}_1 = \widehat{\mathbf{D}}_L \hat{\boldsymbol{\varphi}}_1, \tag{4.13a}$$

$$\Delta^- \hat{\boldsymbol{\varphi}}_J = \widehat{\mathbf{D}}_R \hat{\boldsymbol{\varphi}}_J, \tag{4.13b}$$

where $\widehat{\mathbf{D}}_R = -(\mathbf{P}_4^R)^{-1}\mathbf{P}_3^R$ and $\widehat{\mathbf{D}}_L = -(\mathbf{P}_2^L)^{-1}\mathbf{P}_1^L$. After an inverse $\mathcal{Z}$-transformation the *discrete transparent boundary conditions* read

$$\boldsymbol{\varphi}_1^{n+1} - \boldsymbol{\varphi}_0^{n+1} - \mathbf{D}_L^0 \boldsymbol{\varphi}_1^{n+1} = \sum_{k=1}^{n} \mathbf{D}_L^{n+1-k} \boldsymbol{\varphi}_1^k, \tag{4.14a}$$

$$\boldsymbol{\varphi}_J^{n+1} - \boldsymbol{\varphi}_{J-1}^{n+1} - \mathbf{D}_R^0 \boldsymbol{\varphi}_J^{n+1} = \sum_{k=1}^{n} \mathbf{D}_R^{n+1-k} \boldsymbol{\varphi}_J^k. \tag{4.14b}$$

Remark 4.4. *Note, that in equation (4.13a) and (4.14a) the left boundary condition is given at* $j = 1$*. Of course, the boundary condition can also be formulated at* $j = 0$ *using* $\hat{\boldsymbol{\xi}}_j = \Delta^+ \hat{\boldsymbol{\varphi}}_j$*.*

For a scalar Schrödinger equation Ehrhardt and Arnold showed in [EA01] that the imaginary parts of the coefficients were not decaying but oscillating. Therefore they introduced summed coefficients. These decay rapidly like $O(n^{-3/2})$. We can give no asymptotic behaviour of the systems' coefficients. Therefore, we investigate the coefficients for our example further and compute them numerically (for details see Sec. 5): Their real and imaginary parts are given in Fig. 2 and Fig. 3

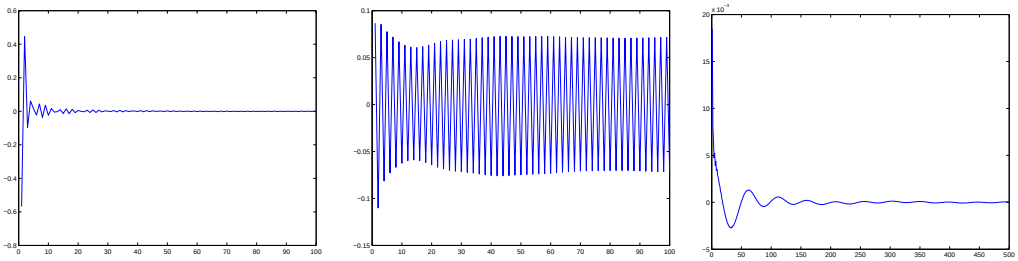

Figure 2: Typical elements of the coefficient matrix $\mathbf{D}_R$: real part of diagonal (left) and off-diagonal elements (type OD1 centre and OD2 right).

respectively. We observe, that the overall behaviour of the diagonal elements is equivalent to that in the scalar case: the real parts decay rapidly, but the imaginary parts alternate without visible decay. This behaviour cannot be found for any off-diagonal element: four off-diagonal elements show an opposite behaviour: for $d_{1,2}^n$,$d_{2,1}^n$,$d_{3,4}^n$ and $d_{4,3}^n$ - these we will call the OD1-type, the remaining off-diagonal elements the OD2-type - the real parts alternate, whereas the imaginary parts decay rapidly. For the OD2-type elements none of the previous behaviour can be observed. They have a much smaller absolute value and decay comparatively slowly. The asymptotic behaviour of the diagonal and four OD1-type elements with alternating imaginary or real parts, suggest the

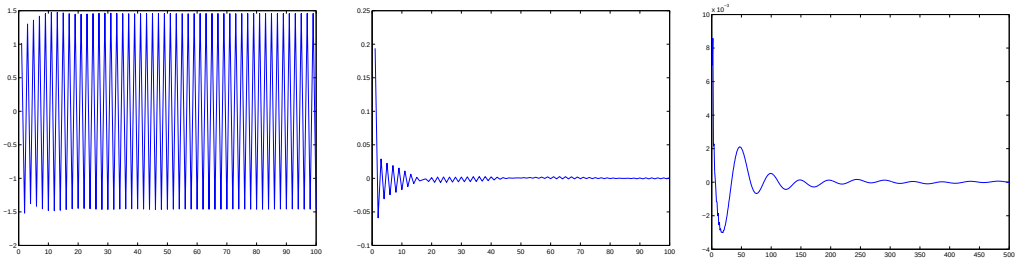

Figure 3: Typical elements of the coefficient matrix $\mathbf{D}_R$: imaginary part of diagonal (left) and off-diagonal elements (type OD1 centre and OD2 right).

use of summed convolution coefficients to avoid subtractive cancellation. With $\widehat{\mathbf{S}}_L = \frac{z+1}{z}\widehat{\mathbf{D}}_L$ and $\widehat{\mathbf{S}}_R = \frac{z+1}{z}\widehat{\mathbf{D}}_R$ the DTBCs with summed coefficients read

$$\boldsymbol{\varphi}_1^{n+1} - \boldsymbol{\varphi}_0^{n+1} - \mathbf{S}_L^0 \boldsymbol{\varphi}_1^{n+1} = \sum_{k=1}^{n} \mathbf{S}_L^{n+1-k} \boldsymbol{\varphi}_1^k - \boldsymbol{\varphi}_1^n + \boldsymbol{\varphi}_0^n, \tag{4.15a}$$

$$\boldsymbol{\varphi}_J^{n+1} - \boldsymbol{\varphi}_{J-1}^{n+1} - \mathbf{S}_R^0 \boldsymbol{\varphi}_J^{n+1} = \sum_{k=1}^{n} \mathbf{S}_R^{n+1-k} \boldsymbol{\varphi}_J^k - \boldsymbol{\varphi}_J^n + \boldsymbol{\varphi}_{J-1}^n. \tag{4.15b}$$

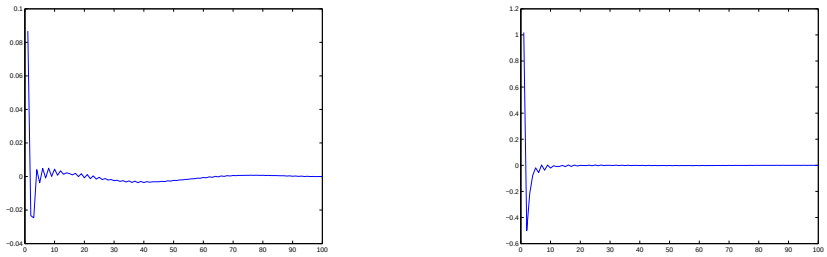

Figure 4: Elements of the summed coefficient matrix $\mathbf{S}_R$: real part of the off-diagonal elements type OD1 (left) and imaginary part of the diagonal element (right).

That this strategy is successful can be seen in the summed convolution coefficients $\mathbf{S}^n$. The real and imaginary parts of the formerly oscillating coefficients are given in Fig. 4: for the diagonal elements and the four OD1-type elements the real parts as well as imaginary parts decay rapidly. The eight slowly decaying OD2-type elements remain unchanged in their qualitative behaviour.

It remains to prove Thm. 4.2. Therefore, we will first show in Lem. 4.2, that no eigenvalue of $\mathbf{A}^{-1}\mathbf{B}+\mathbf{I}$ has an absolute value of one. Then we will show the asserted splitting of the eigenvalues for $\mathbf{M} = 0$ and argue, that due to the continuity of the eigenvalues the border $|\lambda| = 1$ cannot be crossed.

Lemma 4.2. *For $|z| \neq 1$ the matrix $\mathbf{A}^{-1}\mathbf{B} + \mathbf{I}$ has no eigenvalue λ with $|\lambda| = 1$.*

Proof. Assume that $\lambda = a + bi$ with $|\lambda| = 1$ were an eigenvalue of the discrete problem (4.6). Then $\hat{\boldsymbol{\varphi}}_j = \lambda^j \hat{\boldsymbol{\varphi}}_0$ is a solution of (4.6). Inserting $\hat{\boldsymbol{\varphi}}_j = \lambda^j \hat{\boldsymbol{\varphi}}_0$ in equation (4.6) yields with $g(z) = \frac{z-1}{z+1}$:

$$i\frac{2\Delta x^2}{\Delta t} g(z) \lambda \hat{\boldsymbol{\varphi}}_0 = \lambda \left(-\mathbf{m}(a-1) + \mathbf{M}\Delta x b + \Delta x^2 \mathbf{V} \right) \hat{\boldsymbol{\varphi}}_0. \tag{4.16}$$

Thus, either $\lambda = 0$ or equation (4.16) is an eigenvalue equation for the matrix $-\mathbf{m}(a-1) + \mathbf{M}\Delta x b + \Delta x^2 \mathbf{V}$, which is as a sum of Hermitian matrices again Hermitian, and has therefore only real eigenvalues. Thus $i\frac{2\Delta x^2}{\Delta t} g(z)$ must be real. We examine this expression further:

$$g(z) = \frac{z-1}{z+1} = \frac{|z|^2 - 1 + 2i\,\mathrm{Im}(z)}{|z+1|^2}. \tag{4.17}$$

It is obvious, that $g(z) \in i\mathbb{R}$ if and only if $|z| = 1$. □

To understand the eigenvalue-splitting for the general case, i.e. equation (4.6), we shall now use a perturbation argument and consider the special case $\mathbf{M} = \mathbf{0}$. Then equation (4.6) reads

$$2i\frac{\Delta x^2}{\Delta t}\frac{z-1}{z+1}\hat{\boldsymbol{\varphi}}_j = -\mathbf{m}\Delta^+\Delta^-\hat{\boldsymbol{\varphi}}_j + \Delta x^2 \mathbf{V}\hat{\boldsymbol{\varphi}}_j. \tag{4.18}$$

Exchanging the space index $j \to -j$ yields the identical equation. Thus, both problems have the same solutions and the eigenvalues of $\mathbf{A}^{-1}\mathbf{B} + \mathbf{I}$ are in both cases the same. Since decaying solutions are increasing for $j \to -j$ and vice versa, the eigenvalues must split in d yielding decaying and d yielding increasing solutions for $|z| \neq 1$ and $j \to \infty$.

To (4.18) we add the term $i\varepsilon\frac{\Delta x}{2}\mathbf{M}(\Delta^+ + \Delta^-)\boldsymbol{\varphi}$ for $0 \leq \varepsilon \leq 1$. Then Lem. 4.2 shows that no eigenvalue λ can have an absolute value one. Since these eigenvalues are continuous in ε(cf. [HJ99a]), d eigenvalues must remain inside the unit circle when ε varies from 0 to 1 and d eigenvalues stay outside.

This finishes the proof of Thm. 4.2.

4.1 Stability

At the beginning of this section we showed that the l^2-norm of the whole-space problem is constant in time. For the interior scheme with the DTBCs the l^2-norm is bounded by the l^2-norm of the whole-space problem, because the DTBCs cut off the exterior parts of the solution:

$$||\boldsymbol{\varphi}^n||^2_{l^2(0,J)} \leq ||\boldsymbol{\varphi}^n||^2_{l^2(-\infty,\infty)} = ||\boldsymbol{\varphi}^0||^2_{l^2(-\infty,\infty)}. \tag{4.19}$$

Thus the interior scheme with DTBCs constructed from exact convolution coefficients is stable. Since we have to compute the convolution coefficients numerically, this does not work and we consider (4.1) for $j = 0, \ldots, J$, then in the computation of (4.3) there remain some boundary terms due to the summation by parts rule:

$$\begin{aligned}\frac{\Delta x^2}{\Delta t}\triangle_t^+||\boldsymbol{\varphi}^n||^2_{l^2} = \mathrm{Im}\Big((\boldsymbol{\varphi}_0^{n+\frac{1}{2}})^H \mathbf{m}_L \triangle^+ \boldsymbol{\varphi}_0^{n+\frac{1}{2}} + (\boldsymbol{\varphi}_0^{n+\frac{1}{2}})^H \mathbf{M}_{SL}^H \boldsymbol{\varphi}_0^{n+\frac{1}{2}} \\ + (\boldsymbol{\varphi}_J^{n+\frac{1}{2}})^H \mathbf{m}_R \triangle^- \boldsymbol{\varphi}_J^{n+\frac{1}{2}} + (\boldsymbol{\varphi}_J^{n+\frac{1}{2}})^H \mathbf{M}_{SR}^H \boldsymbol{\varphi}_J^{n+\frac{1}{2}}\Big).\end{aligned} \tag{4.20}$$

As differences we rather consider $\triangle^+$ and $\triangle^-$ than $\triangle^0_{\frac{\Delta x}{2}}$. This is possible, since at the boundaries the coefficient matrix $\mathbf{m}$ is already constant. Thus, if (4.20) is non-positive the Crank-Nicolson scheme with DTBCs is stable. Unfortunately, inserting the DTBCs for the differential terms does not help to show this, because we know too little of the properties of the convolution matrices. Instead, we will perform a numerical evaluation of the boundary terms and thus numerically test

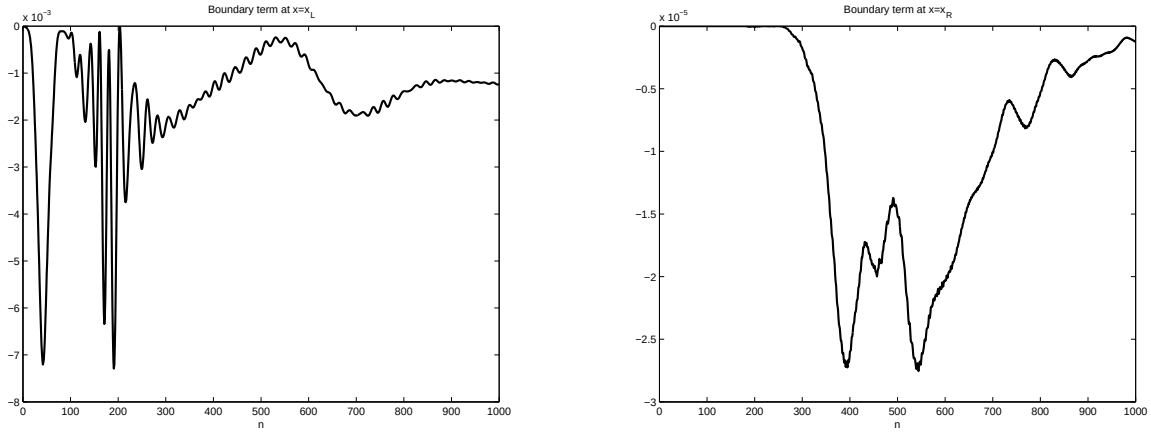

Figure 5: Time dependent behaviour of the stability terms of (4.20) at the left and right boundary

the stability for our example: In Fig. 5 we give the terms in (4.20) for the left and right boundary. We observe, that they keep the correct sign strictly. If we change the initial condition in that way, that the wave packages travel to the left, i.e. choosing a negative k_r, exchanges the behaviour of the left and right boundary terms.

5 The computation of the convolution coefficients with the numerical inverse $\mathcal{Z}$-transformation

The $\mathcal{Z}$-transformation (or in the analytical part the Laplace-transformation) is the mighty instrument, which enables us to solve occurring equations and to formulate this kind of transparent boundary conditions. In the implementation the numerical inverse $\mathcal{Z}$-transformation proved to be a more subtle problem than every other point including e.g. the calculation of eigenvectors. For that reason, we will investigate it further.

5.1 Performing $\mathcal{Z}$-transformation with Fourier-transformation

Many mathematical toolboxes contain ordinary transformations, including a (fast) Fourier-transformation as a standard routine. The less common $\mathcal{Z}$-transformation is rarely found. Here, we will present the easy coherence between both. The $\mathcal{Z}$-transform will be denoted by $\mathcal{Z}$, F is the discrete Fourier-transform. On the unit circle holds for the *finite $\mathcal{Z}$-transform* $\mathcal{Z}^N$ for $z = e^{i\varphi}$

$$\mathcal{Z}(f_j) \approx \mathcal{Z}^N(f_j) = \sum_{j=0}^{N} f_j z^{-j} = \sum_{j=0}^{N} f_j e^{-ij\varphi} = F(e^{i\varphi}). \tag{5.1}$$

On a circle with radius r holds

$$F(re^{i\varphi}) = \sum_{j=0}^{N} f_j r^{-j} e^{-ij\varphi} = \sum_{j=0}^{N} f_j r^{-j} z^{-j} = \mathcal{Z}^N(f_j r^{-j}) \approx \mathcal{Z}(f_j r^{-j}). \tag{5.2}$$

We observe, that applying the inverse $\mathcal{Z}$-transformation not on the unit circle necessitates a rescaling of the n-th convolution coefficient with r^n. For big circles this causes numerical problems.

5.2 The error of the numerical inverse $\mathcal{Z}$-transformation

In this section we will examine the numerical error caused by the inverse $\mathcal{Z}$-transformation, since it is the crucial point in the numerical implementation. For the transformation we have to choose a radius r and a number N of points z_k to define the circle on which the transformation is performed. An intelligent choice of these parameters is essential to achieve good results.

The numerical error can be separated in ε_{approx} the error in the approximation on a finite number of sampling points and the roundoff error ε_{round}. We will inverse $\mathcal{Z}$-transform the function $\hat{\ell}$ (representing either a coefficient $\hat{d}_{s,l}$ or a summed coefficient $\hat{s}_{s,l}$), yielding the series ℓ_n. ℓ_n^N denotes the approximation on a circle with N sampling points. A tilde on top of it indicates that the roundoff error is considered.

The $\mathcal{Z}$-transformation of $\{\ell_m\}$ at the sampling points z_k reads

$$\hat{\ell}_k := \hat{\ell}(z_k) = \sum_{m=0}^{\infty} \ell_m z_k^{-m}, \qquad \text{with } z_k = re^{-ik\frac{2\pi}{N}}. \tag{5.3}$$

If we assume, that $\hat{\ell}(z)$ is an analytic function for $|z| > R$, then the ℓ_n are just identical with the Laurent coefficients of $\hat{\ell}(z)$ given by

$$\ell_n = \frac{1}{2\pi i} \oint_{S_\rho} \hat{\ell}(z) z^{n-1} dz, \tag{5.4}$$

where S_ρ denotes the sphere with radius $\rho > R$. If we substitute $z = \rho e^{i\varphi}$, we obtain

$$\ell_n = \frac{\rho^n}{2\pi} \int_0^{2\pi} \hat{\ell}\left(\rho e^{i\varphi}\right) e^{in\varphi} d\varphi. \tag{5.5}$$

Defining $Q_{\hat{\ell}}^{\rho} = \max\limits_{0\le\varphi\le 2\pi} \left|\hat{\ell}\left(\rho e^{i\varphi}\right)\right|$ gives the estimate

$$|\ell_n| \le \rho^n Q_{\hat{\ell}}^{\rho}. \tag{5.6}$$

The inverse $\mathcal{Z}$-transformation of $\hat{\ell}$ can be approximated on N discrete sampling points as follows

$$\ell_n^N = \frac{1}{N} r^n \sum_{k=0}^{N-1} \hat{\ell}_k \, e^{ink\frac{2\pi}{N}}, \quad n = 0, \dots N-1. \tag{5.7}$$

We insert (5.3) in (5.7), change the order of summation and use the orthogonality property

$$\begin{aligned}
\ell_n^N &= \frac{1}{N} r^n \sum_{m=0}^{\infty} \ell_m r^{-m} \sum_{k=0}^{N-1} e^{-imk\frac{2\pi}{N}} e^{ink\frac{2\pi}{N}} \\
&= \frac{1}{N} r^n \sum_{m=0}^{\infty} \ell_m r^{-m} \begin{cases} N & \text{, if } m = n + jN \quad , j \in \mathbb{N} \\ 0 & \text{, else} \end{cases} \\
&= r^n \sum_{k=0}^{\infty} \ell_{n+kN} \, r^{-(n+kN)}.
\end{aligned}$$

This gives

$$\ell_n^N - \ell_n = \sum_{k=1}^{\infty} \ell_{n+kN} \, r^{-kN}. \tag{5.8}$$

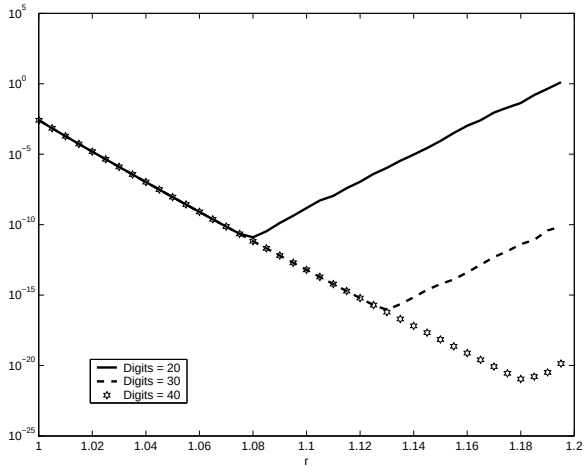

Figure 6: Error in one element of the matrix $\mathbf{D}$

Now, we insert inequality (5.6) in (5.8) and sum the geometric series, which yields

$$|\ell_n^N - \ell_n| \leq \rho^n Q_{\hat{\ell}}^{\rho} \sum_{k=1}^{\infty} \left(\frac{\rho}{r}\right)^{kN} = \rho^n Q_{\hat{\ell}}^{\rho} \frac{\left(\frac{\rho}{r}\right)^N}{1 - \left(\frac{\rho}{r}\right)^N} \tag{5.9}$$

for $r > \rho > R$.

Similar estimates have been derived in the application of quadrature rules to numerical integration by Lubich, which involve Fourier transformation (cf. [Lub88], [Hen79]).

The other influential error is the roundoff error, that depends on the machine accuracy ε_m and the accuracy ε in the numerical computation of $\hat{\ell}_k$. For instance, we will use $\tilde{a} = a(1 + \varepsilon_m)$ as the computer representation of an exact value a. The roundoff error of the inverse $\mathcal{Z}$-transformation is calculated from equation (5.7). The main part results from the N fold summation of $\hat{\ell}_k$ and the exponential function.

$$\left|\tilde{\ell}_n^N - \ell_n^N\right| \leq r^n \left(CN\varepsilon_m + \varepsilon\right) Q_{\hat{\ell}_k}^r \tag{5.10}$$

Together with (5.9) the error is bounded by

$$|\tilde{\ell}_n^N - \ell_n| \leq \rho^n Q_{\hat{\ell}}^{\rho} \frac{\left(\frac{\rho}{r}\right)^N}{1 - \left(\frac{\rho}{r}\right)^N} + r^n \left((N+1)\varepsilon_m + \varepsilon\right) Q_{\hat{\ell}_k}^r + O(\varepsilon_m^2 + \varepsilon\varepsilon_m). \tag{5.11}$$

It is possible to show this behaviour of the error roughly in numerical examples. We calculated the series $\mathbf{D}^n$ for the quantum well problem with different accuracy (20, 30 and 40 digits precision) and considered the solution obtained with 50 digits precision as a reference solution. We used $N = 256$ sampling points on the circle. The Euclidean norm of the error is shown in Fig. 6 for one of the 16 entries in the matrix $\mathbf{D}$. For all entries the error figure has the same behaviour: the error decreases with growing radius, up to a r_{opt}, after which the roundoff error grows rapidly. Observe, that the y-axis of the plot is in logarithmic scale. The curves for 20, 30 and 40 digits coincide for small values of r up to the radius r_{opt}^{20}, r_{opt}^{30} respectively.

Since the calculation for a system is rather expensive, it is desirable to predict a radius close to r_{opt}. For the different entries in $\mathbf{D}$ the optimal radius varies but slightly - up to a difference of 0.001.

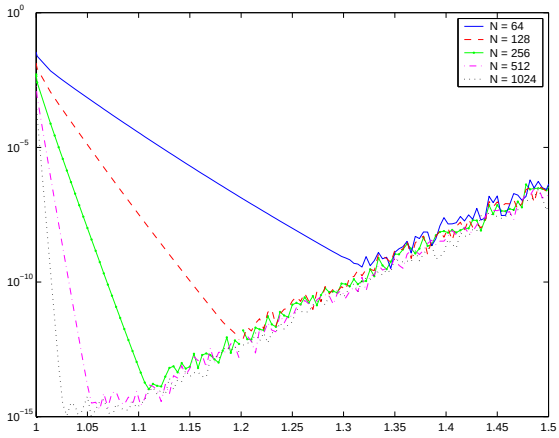

Figure 7: Error in one element of the matrix $\mathbf{D}$ calculated with 20 digits precision depending on the number N of sampling points for the inverse $\mathcal{Z}$-transformation

The preceeding figure showed the influence of the mantissa length on the accuracy of the calculation. Now, we want to show the dependence of the error on the number N of sampling points. Fig. 7 shows five error curves with 20 digits precision; one for N= 64, 128, 256, 512 and 1024 respectively. The Euclidean norm of the error is summed up to 64. A higher number of sampling points yields a faster decreasing error, r_{opt} becomes smaller and of course the error at r_{opt} becomes less. An influence of N on the round off error is hardly discernable. Comparing the errors at the different N-depending r_{opt}, we notice, that the gain of taking the double number of points gets less with increasing N. Of course the error cannot become less than the precision in the calculation of $\hat{\ell}_n$.

In Fig. 8 we compare the error in the Euclidean norm with the error bound (5.11), i.e. with the separate bounds for the approximation error and roundoff error. We assumed $\varepsilon = 10 \cdot \varepsilon_m$ and calculated the maximum of $\hat{\ell}$ on all r for simplicity reasons.

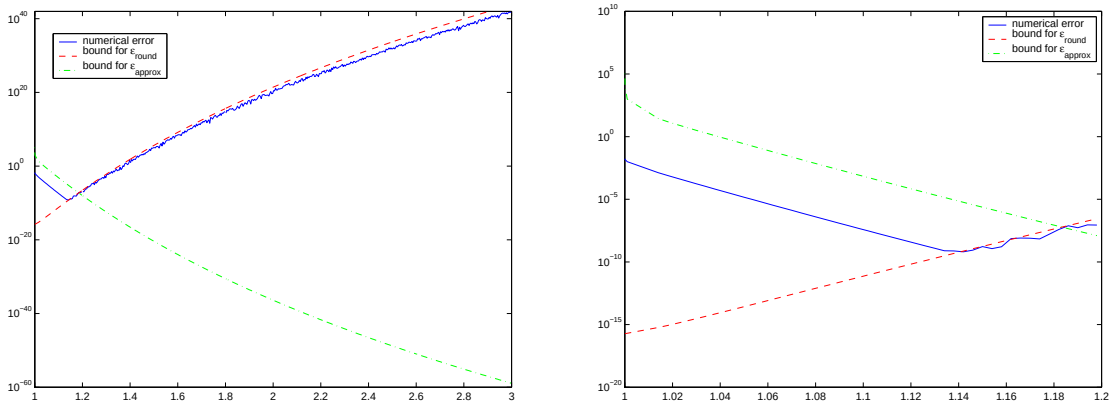

Figure 8: Error and error bounds

We compute the matrices $\hat{\mathbf{D}}$ and $\hat{\mathbf{S}}$ with MATLAB with an accuracy of $\varepsilon = 10^{-16}$. Thus, with a radius $r = 1.018$ and $N = 2^{12}$ sampling points, we achieve an accuracy of 10^{-8}.

6 The sum of exponentials ansatz and the fast evaluation of the convolution

In order to reduce the numerical effort due to the boundary condition below that of the overall scheme, it is necessary to make some kind of approximation. We focus on the convolution coefficients: But the simple approach to cut off the convolution after a constant number of summands yields bad results. In this section we will use the approach of Arnold, Ehrhardt and Sofronov [AES03] to approximate the coefficients $\widetilde{s}^n_{s,l}$ by the *sum of exponentials* ansatz. Afterwards we explain how these approximated convolution coefficients $\widetilde{a}^n_{s,l}$ enable us to fast evaluate the discrete convolution.

6.1 The sum of exponentials ansatz

The approximation has to be done for each element in $\mathbf{S}$ separately. We use for each $s, \tau = 1, \ldots, S$ the following ansatz, which uses a sum of exponentials

$$\widetilde{s}^n_{s,\tau} \approx \widetilde{a}^n_{s,\tau} := \begin{cases} \widetilde{s}^n_{s,\tau}, & n = 0, \ldots, \nu - 1 \\ \sum\limits_{l=1}^{L(s,\tau)} g_{s,\tau,l}\, h^{-n}_{s,\tau,l}, & n = \nu, \nu+1, \ldots, \end{cases} \tag{6.1}$$

where $L(s,\tau) \in \mathbb{N}$ and $\nu \geq 0$ are fixed numbers. The approximation quality of this ansatz depends on $L(s,\tau)$, ν and the sets $\{g_{s,\tau,l}\}$ and $\{h_{s,\tau,l}\}$ for all $s, \tau = 1, \ldots, S$.

In the following we present a method to calculate these sets for given $L(s,\tau)$ and ν. We consider the formal power series

$$f_{s,\tau}(x) := \widetilde{s}^{\nu}_{s,\tau} + \widetilde{s}^{\nu+1}_{s,\tau} x + \widetilde{s}^{\nu+2}_{s,\tau} x^2 + \ldots, \qquad \text{for } |x| \leq 1. \tag{6.2}$$

If the Padé approximation of (6.2)

$$\tilde{f}_{s,\tau}(x) := \frac{n^{(L(s,\tau)-1)}_{s,\tau}(x)}{d^{(L(s,\tau))}_{s,\tau}(x)} \tag{6.3}$$

exists (where the numerator and the denominator are polynomials of degree $L(s,\tau)-1$ and $L(s,\tau)$ respectively), then its Taylor series

$$\tilde{f}_{s,\tau}(x) = \widetilde{a}^{\nu}_{s,\tau} + \widetilde{a}^{\nu+1}_{s,\tau} x + \widetilde{a}^{\nu+2}_{s,\tau} x^2 + \ldots \tag{6.4}$$

satisfies the conditions

$$\widetilde{a}^n_{s,\tau} = \widetilde{s}^n_{s,\tau}, \qquad \text{for } n = \nu, \nu+1, \ldots, 2L(s,\tau) + \nu - 1 \tag{6.5}$$

according to the definition of the Padé approximation rule.

We now consider, how to compute the coefficient sets $\{g_{s,\tau,l}\}$ and $\{h_{s,\tau,l}\}$.

Theorem 6.1 ([AES03], Theorem 3.1.). *Let $d^{L(s,\tau)}_{s,\tau}$ have $L(s,\tau)$ simple roots $h_{s,\tau,l}$ with $|h_{s,\tau,l}| > 1$, $l = 1, \ldots, L(s,\tau)$. Then*

$$\widetilde{a}^n_{s,\tau} = \sum_{l=1}^{L(s,\tau)} g_{s,\tau,l}\, h^{-n}_{s,\tau,l}, \qquad n = \nu, \nu+1, \ldots, \tag{6.6}$$

where

$$g_{s,\tau,l} := -\frac{n_{s,\tau}^{(L(s,\tau)-1)}(h_{s,\tau,l})}{\left(d_{s,\tau}^{(L(s,\tau))}\right)'(h_{s,\tau,l})}\, h_{s,\tau,l}^{\nu-1} \neq 0, \qquad l = 1, \ldots, L(s,\tau). \tag{6.7}$$

Remark 6.2. *The asymptotic decay of the $\widetilde{a}_{s,\tau}^n$ is exponential. This is due to the sum of exponentials ansatz* (6.1) *and the assumption $|h_{s,\tau,l}| > 1$, $l = 1, \ldots, L(s,\tau)$.*

The above analysis permits us to give the following description of the approximation to the convolution coefficients by the representation (6.1) if we use a $[L(s,\tau)-1|L(s,\tau)]$ Padé approximant to (6.2): the first $2L(s,\tau) + \nu - 1$ coefficients are reproduced exactly, see (6.5); however, the asymptotic behaviour of $\widetilde{s}_{s,\tau}^n$ and $\widetilde{a}_{s,\tau}^n$ (as $n \to \infty$) differs strongly (algebraic versus exponential decay).

We note that the Padé approximation must be performed with high precision ($2L(s,\tau)-1$ digits mantissa length) to avoid a 'nearly breakdown' by ill conditioned steps in the Lanczos algorithm (cf. [BB97]). If such problems still occur or if one root of the denominator is smaller than 1 in absolute value, the orders of the numerator and denominator polynomials are successively reduced. In our numerical test case we started with $L(s,\tau) \equiv 30$ and except from two outlier values the finally reached values of $L(s,\tau)$ were between 25 and 30. Fig. 9 shows the error $|\widetilde{s}_{s,\tau}^n - \widetilde{a}_{s,\tau}^n|$ versus n for the outlier with $L(1,2) = 15$ for the imaginary part of $\widetilde{s}_{1,2}^n$ (left) and with $L(2,2) = 30$ for the real part of $\widetilde{s}_{2,2}^n$ (right). Observe, that both plots are in logarithmic scale. Clearly, the error increases significantly for $n > 2L(s,\tau) + 1$.

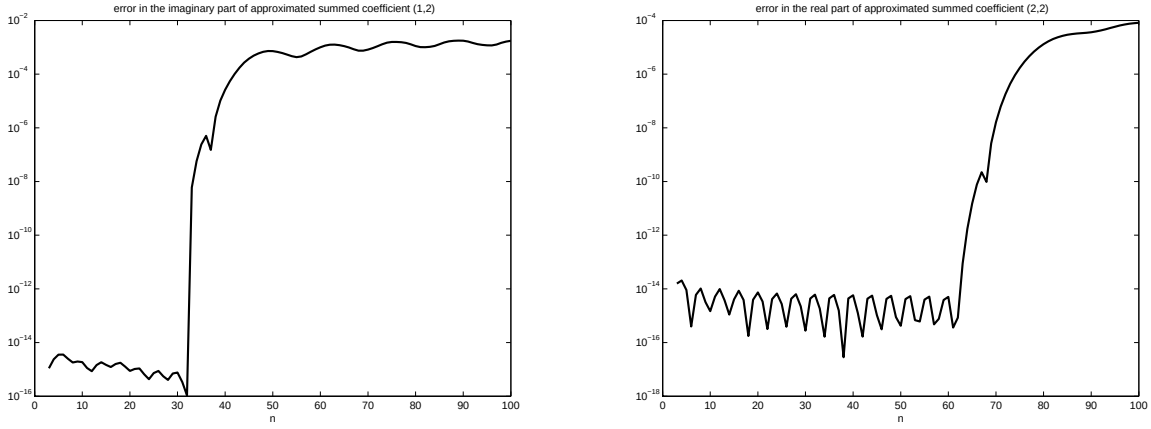

Figure 9: Error $|\widetilde{s}_{s,\tau}^n - \widetilde{a}_{s,\tau}^n|$ versus n: imaginary part for $s = 1, \quad \tau = 2$ (left) and real part for $s = \tau = 2$ (right)

6.2 The fast evaluation of the approximate convolution

Now we describe the fast evaluation of the discrete approximate convolution. The convolution

$$C_{s,\tau}^{(n+1)}(u) := \sum_{k=1}^{n+1-\nu} \widetilde{a}_{s,\tau}^{n+1-k}\, u_{\tau,J}^k, \tag{6.8}$$

with

$$\widetilde{a}_{s,\tau}^n := \sum_{l=1}^{L(s,\tau)} g_{s,\tau,l}\, h_{s,\tau,l}^{-n}, \qquad n = \nu, \nu+1, \ldots \tag{6.9}$$

can be calculated efficiently by a simple recurrence formula:

Theorem 6.3 ([AES03], Theorem 4.1.).

$$C_{s,\tau}^{(n+1)}(u) = \sum_{l=1}^{L(s,\tau)} C_{s,\tau,l}^{(n+1)}(u) \tag{6.10}$$

with

$$\begin{aligned} C_{s,\tau,l}^{(n+1)}(u) &= h_{s,\tau,l}^{-1} C_{s,\tau,l}^{(n)} + g_{s,\tau,l} h_{s,\tau,l}^{-\nu} u_{\tau,J}^{n+1-\nu}, \qquad n = \nu, \nu+1, \dots \\ C_{s,\tau,l}^{(\nu)}(u) &\equiv 0 \end{aligned} \tag{6.11}$$

Finally, we summarise the above method to evaluate approximate DTBCs:

Step 1: For each s, τ choose $L(s,\tau)$ and ν and calculate the exact convolution coefficients $\widetilde{s}_{s,\tau}^n$ for $n = 0, \dots, 2L(s,\tau) + \nu - 1$.

Step 2: For each s, τ use the Padé approximation (6.3) for the series (6.4) with $\widetilde{a}_{s,\tau}^n = \widetilde{s}_{s,\tau}^n$, for $n = \nu, \nu+1, \dots, 2L(s,\tau)+\nu-1$ to calculate the sets $\{g_{s,\tau,l}\}$ and $\{h_{s,\tau,l}\}$ for all $s, \tau = 1, \dots, S$ according to Theorem 6.1.

Step 3: Implement the recurrence formulas (6.10), (6.11) to calculate the approximate convolutions.

7 Numerical results

In this section we present the numerical results for simulating the transient behaviour of the quantum well with the data of Sec. 2.1. Fig. 10 shows the time dependent behaviour of the first two components $\varphi_{1,j}$ (solid) and $\varphi_{2,j}$ (dashed). We concentrate on the first two components, since there is less mass in component three and four. The initial Gaussian wave packet (2.4) (in the second component) moves to the right and fragments in two. When the faster wave packet reaches the first barrier, it is partly reflected and partly transmitted. With advancing time some part of the density accumulates between the barriers and is slowly transmitted through the second barrier, then leaving the domain of computation. The part of the density, which is reflected at the first barrier moves on to the left and after a time, where the wave packages superpose each other, it moves again in form of a Gaussian wave package to the left boundary of the computational domain. The slower wave package seems not to recompose smoothly.

In Fig. 11 we present the relative ℓ^2–error $e_L(t) = \|\boldsymbol{\varphi} - \boldsymbol{\varphi}_a\|_2 / \|\boldsymbol{\varphi}(.,0)\|_2$, where $\boldsymbol{\varphi}_a$ denotes the approximate solution obtained with the approximated DTBCs. $\boldsymbol{\varphi}$ is the solution calculated with exact DTBCs. In our example we used $L(s,\tau) = 30$ initially. One observes that the error is increasing (due to the interaction with the potential) but still remains after 1000 time steps below $6 \cdot 10^{-3}$. The zoomed region shows the l^2-error of the solution for the first 60 time steps, where the upper bound is 10^{-5}.

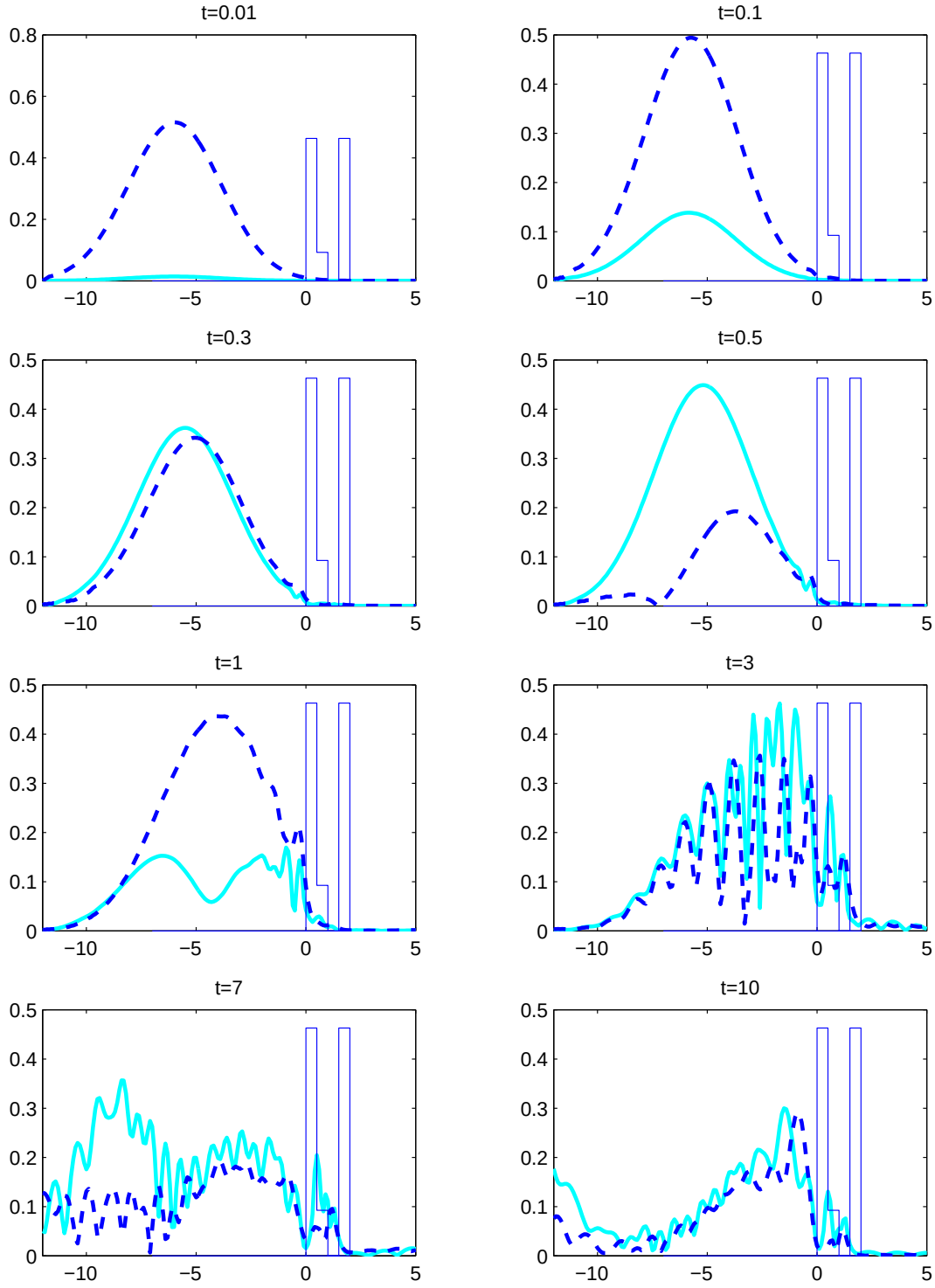

Figure 10: Time dependent behaviour of $\varphi_{1,j}$ (solid) and $\varphi_{2,j}$ (dashed).

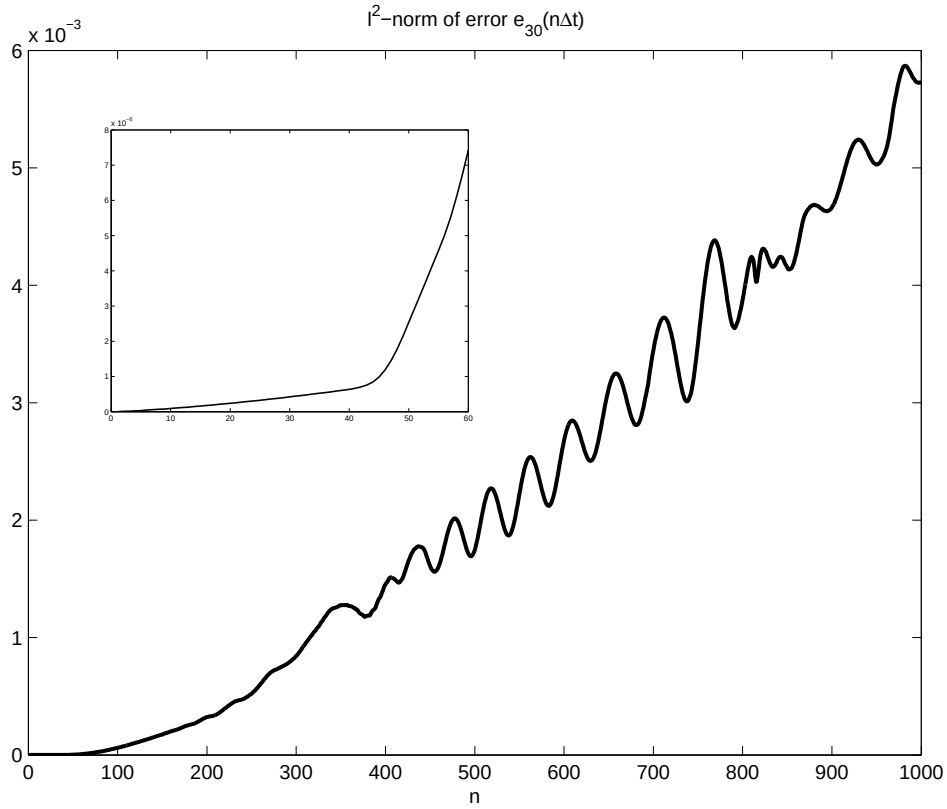

Figure 11: l2-error of the solution with approximated coefficients

8 Conclusions and perspectives

In this paper we showed the mathematical background for a discrete transparent boundary condition for one-dimensional *kp*-Schrödinger equations in detail and approximated the DTBC by a sum of exponentials ansatz. We illustrated by a simple example the quality of these DTBCs. In a succeeding paper, we will concentrate on the analysis of the tunneling properties of a real quantum-well structure using this tool and calculating physical parameters as charging and escape times. Additionally we will be concerned with the stationary case.

Acknowledgement

The first two authors were partially supported by the DFG Priority Program Analysis, Modeling and Simulation of Multi-Scale Problems under Grant-No. AR 277/3-2. The work of Th. Koprucki was supported by the same DFG Priority Program under Grant FU 316/5-2.

The first and third author were supported by the DFG Research Center "Mathematics for key technologies" (FZT 86) in Berlin.

References

[AES03] A. Arnold, M. Ehrhardt, and I. Sofronov. Discrete transparent boundary conditions for the Schrödinger equation: Fast calculation, approximation, and stability. *Comm. Math. Sci.*, 1(3):501–556, 2003.

[Arn98] A. Arnold. Numerically Absorbing Boundary Conditions for Quantum Evolution Equations. *VLSI Design*, 6:313–319, 1998.

[BAM98] A.C. Rodrigues Bittencourt, A.M.Cohen, and G.E. Marques. Strain-indused enhancement of resonant current of holes in multilayered heterostructures. *Phys. Rev. B*, 57(8):4525–4543, 1998.

[Bas88] G. Bastard. *Wave Mechanics Applied to Semiconductor Heterostructures.* Hasted Press, 1988.

[BB97] A. Bultheel and M. Van Barel. *Linear algebra, rational approximation and orthogonal polynomials.* Studies in Computational Mathematics 6. North-Holland, 1997.

[BKKR00] U. Bandelow, H.-Chr. Kaiser, Th. Koprucki, and J. Rehberg. Spectral properties of $k \cdot p$ Schrödinger operators in one space dimension. *Numer. Funct. Anal. Optimization*, 21(3-4):379–409, 2000.

[Bur92] M. G. Burt. The justification for applying the effective-mass approximation to microstructures. *J. Physics. Condens. Matter*, 4:6651–6690, 1992.

[Bur94] M. G. Burt. Direct derivation of effective-mass equations for microstructures with atomically abrupt boundaries. *Phys. Rev. B*, 50(11):7518–7525, 1994.

[Bur98] M. G. Burt. Fundementals of envelope function theory for electronic states and photonic modes in nanostructures. *J. Physics. Condens. Matter*, 11:R53–R83, 1998.

[Car96] M. Cardona. *Fundamentals of Semiconductors.* Springer-Verlag, Berlin, 1996.

[CC92] C. Y.-P. Chao and S. L. Chuang. Spin-orbit-coupling effects on the valence-band structure of strained semiconductor quantum wells. *Phys. Rev. B*, 46(7):4110–4122, 1992.

[Chu91] S. L. Chuang. Efficient band-structure calculations of strained quantum wells. *Phys. Rev. B*, 43(12):9649–9661, 1991.

[Chu95] S. L. Chuang. *Physics of optoelectronic Devices.* Wiley & Sons, New York, 1995.

[CS63] D. Carlson and H. Schneider. Inertia theorems for matrices: The semidefinite case. *J. Math. Anal. Appl.*, 6:430–446, 1963.

[DF93] P. Debernardi and P. Fasano. Quantum Confined Stark Effect in Semiconductor Quantum Wells Including Valence Band Mixing and Coulomb Effects. *IEEE J. Quantum Electronics*, 29(11):2741–2755, 1993.

[EA01] M. Ehrhardt and A. Arnold. Discrete transparent boundary conditions for the Schrödinger equation. *Riv. Mat. Univ. Parma*, 6:57–108, 2001.

[Hen79] P. Henrici. Fast Fourier Methods in Computational Complex Analysis. *SIAM Review*, 21(4):481–527, 1979.

[HJ99a] R. A. Horn and Ch. R. Johnson. *Matrix Analysis*. Cambridge University Press, 1999.

[HJ99b] R. A. Horn and Ch. R. Johnson. *Topics in Matrix Analysis*. Cambridge University Press, 1999.

[Kan82] E. O. Kane. Energy Band Theory. In W. Paul, editor, *Handbook on Semiconductors*, volume 1, chapter 4a, pages 193–217. North-Holland, Amsterdam, New York, Oxford, 1982.

[Lev00] M. Levy. *Parabolic equation methods for electromagnetic wave propagation*, volume 45 of *IEE: Electromagnetic waves series*. The institution of electrical Engineers, 2000.

[Lub88] C. Lubich. Convolution Quadrature and Discretized Operational Calculus II. *Numer. Math.*, 52:413–425, 1988.

[MGO94] A. T. Meney, Besire Gonul, and E. P. O'Reilly. Evaluation of various approximations used in the envelope-function method. *Phys. Rev. B*, 50(15):10893–10904, 1994.

[SH91] J.A. Stovneng and E.H. Hauge. Time-dependent resonant tunneling of wave packets in the tight-binding model. *Phys. Rev. B*, 44(24), 1991.

[Sin93] J. Singh. *Physics of semiconductors and their heterostructures*. McGraw–Hill, New York, 1993.

[SKB+98] C. Sirtori, P. Kruck, S. Barbieri, Ph. Collot, J. Nagle, M. Beck, J. Faist, and U. Oesterle. $GaAs/Al_xGa_{1-x}As$ quantum cascade lasers. *Appl. Phys. Lett.*, 73(24):3486–3488, 1998.

[SS91] V. Sankaran and J. Singh. Formalism for tunneling of mixed-symmetry electronic states: Application to electron and hole tunneling in direct- and indirect-band-gap $GaAs/Al_xGa_{1-x}As$ structures. *Phys. Rev. B*, 44(7):3175–3186, 1991.

[WM93] M. Wagner and H. Mizuta. Complex-energy analysis of intrinsic lifetimes of resonances in biased multiple quantum wells. *Phys. Rev. B*, 48(19):14393–14406, 1993.

[ZG91] J. Zhang and B. Gu. Temporal characteristics of electron tunneling in double-barrier stepped quantum-well structures. *Phys. Rev. B*, 43(6):5028–5034, 1991.